water

MDPI

Article

Evolution of the Groundwater Flow System since the Last Glacial Maximum in the Aksu River Basin (Northwest China)

Hu Su [1], Yinger Deng [1,*], Weihua Nai [2], Rui Zhang [3], Jihan Huang [4], Pengjie Li [1], Hongkun Yang [1], Lin Chen [1] and Ning Wang [1]

[1] College of Environment and Civil Engineering, Chengdu University of Technology, Chengdu 610059, China; suhugeology@163.com (H.S.); pengjielee007@outlook.com (P.L.); yhk277401@163.com (H.Y.); chenlin985211@outlook.com (L.C.); cdboshi2020@126.com (N.W.)
[2] No. 2 Hydrological and Engineering Geology Party of Xinjiang Bureau of Geology and Mineral Resources Exploration and Development, Changji 831100, China; 13579058681@163.com
[3] College of Urban and Environmental Sciences, Hubei Normal University, Huangshi 435002, China; zhangrui@hbnu.edu.cn
[4] TBEA Co., Ltd., Changji 831100, China; hjh0607@126.com
* Correspondence: cdutgeology2008@126.com

Abstract: Thoroughly investigating the evolution of groundwater circulation and its controlling mechanism in the Aksu River Basin, where human activities are intensifying and the groundwater environment is increasingly deteriorating, is highly urgent and important for promoting the theory, development and implementation of groundwater flow systems (GFSs) and protecting groundwater resources. Based on a detailed analysis of the sediment grain size distribution, chronology, electrofacies, glacial sedimentary sequence, palaeoclimate indicators and existing groundwater age, this paper systematically reconstructs the palaeosedimentary environment of the basin-scale aquifer system in the study area and scientifically reveals the evolutionary pattern and formation mechanism of the GFS. The results showed that the later period of the late Pleistocene experienced a rapid downcutting erosional event caused by tectonic uplift, and the sedimentary environment transitioned from a dry–cold deep downcutting environment in the Last Glacial Maximum (LGM) to a coarse-grained fast-filling fluvial facies sedimentary environment in the Last Glacial Deglaciation (LDP) as the temperature rose; then, it shifted to an environment of fine-grained stable alternating accumulation of fluvial facies and lacustrine facies that was dominated by the warm and arid conditions of the Holocene megathermal period (HMP); this process changed the previous river base level via erosion, glacier elongation or shortening and river level, thus resulting in a complex coupling relationship between the palaeosedimentary environment, palaeoclimate and basin GFS. Furthermore, the existing GFS pattern in the basin exhibits a vertically unconformable groundwater age distribution, which indicates that it is the outcome of the complex superposition of groundwater flow controlled by the palaeosedimentary environment in different periods. Therefore, neotectonic movement and climate fluctuation have jointly acted on the variation in the river level, resulting in the "seesaw" effect, thereby fundamentally controlling the strength of the driving force of groundwater and resulting in the gradual evolution of the GFS from the fully developed regional GFS pattern during the LGM to the current multihierarchy nested GFS pattern.

Keywords: groundwater flow system; evolution; palaeoenvironment; palaeoclimate; Last Glacial Maximum; Aksu River Basin; Xinjiang China

Citation: Su, H.; Deng, Y.; Nai, W.; Zhang, R.; Huang, J.; Li, P.; Yang, H.; Chen, L.; Wang, N. Evolution of the Groundwater Flow System since the Last Glacial Maximum in the Aksu River Basin (Northwest China). *Water* **2023**, *15*, 3459. https://doi.org/10.3390/w15193459

Academic Editor: Adriana Bruggeman

Received: 12 September 2023
Revised: 27 September 2023
Accepted: 28 September 2023
Published: 30 September 2023

1. Introduction

The evolution of the Quaternary sedimentary environment and Quaternary climate change in the Tarim Basin is greatly significant to deep-earth, deep-time studies of the Tibetan Plateau uplift, the formation of environmental patterns in basins in northwest China and the environment of occurrence and flow characteristics of groundwater resources

in the basins [1,2]. The interaction of multiple environmental elements during geologic history has resulted in an orderly spatial and temporal distribution of various components in groundwater [3,4], and groundwater is often regarded as a carrier of information on the evolution of the geologic environment [5]. The Aksu River Basin has extremely thick Quaternary sediments, complex lithofacies, diverse genetic lithofacies types and relatively abundant surface water and groundwater resources; the basin contains a large amount of Quaternary geological, climatological, environmental evolutionary and groundwater resource information, making it an ideal place to study the palaeoenvironment, palaeoclimate, neotectonic movement, sedimentary response and aquifer system in the Tarim Basin and even the whole arid area of western China. In addition, as urbanization has developed and human activities have intensified, China has begun facing a series of tricky problems, such as overexploitation of groundwater resources [6], less advanced irrigation systems and methods, frequent and rapid fluctuations in groundwater levels, soil salinization, desertification, and flash floods; these issues, coupled with the distribution of primary poor-quality groundwater, many underground projects and the construction of various waste accumulation sites [7], has resulted in the deterioration of the groundwater environment and ecological balance [8–10]. Therefore, there is an urgent need to carry out comprehensive research on the sedimentary framework of the basin and the evolution of the groundwater flow system since the Quaternary period, to protect coupling systems related to groundwater (including the groundwater water system, geological engineering system, environmental geological disaster system, ecological circulation system, etc.), simulate groundwater flow and guide the comprehensive utilization of water resources.

The theory of groundwater flow systems (GFSs) describes a basin-scale hierarchically nested structure that is determined by physiography, hydrogeologic conditions and anthropogenic activity [11,12]. The main factors controlling the groundwater flow system include regional topography (Figure 1), development of the morphology of the basin basement, geological structural evolution, stratum (aquifer system) distribution, groundwater-level dynamics and recharge intensity, and human activities, which are largely affected by the sedimentary environment, climatic conditions and tectonic uplift [13–15]. Zhang et al. (1997) [16] discussed the evolution of the Quaternary groundwater system in the North China Plain under the conditions of overexploitation through groundwater dynamic field analysis, groundwater geochemical simulation, ^{14}C dating and isotope information extraction. Zhang et al. (2013) [17] reconstructed the evolution of the Quaternary groundwater flow pattern in the Hebei Plain since the LGM by analyzing the regional physical geography and geological history, and based on environmental isotopes and late changes in continental salinization and saltwater; they concluded that the groundwater flow system of the Hebei Plain is a four-dimensional assemblage of groundwater flow systems in different evolutionary periods, and similar evolutionary histories may occur in other coastal plains and even inland basins where erosion intensity weakens over time. Based on the evolution of the groundwater flow system driven by the sedimentary environment of the Quaternary aquifer system in the Jianghan Plain, Liang et al. (2020) [18] and Zhang et al. (2022a) [19] proposed a developmental and evolutionary history of regional multihierarchical nested GFSs in the basin, which has provided us with a very good case analysis.

There is still a gap in research on the GFS in the periphery of the Tarim Basin, but many studies on the Quaternary stratigraphy, sedimentary environment and climate change have been carried out. Based on a study of the Quaternary magnetostratigraphy of the KT2 borehole in the hinterland, the framework of the stratigraphic sedimentary cycle and palaeoclimatic evolutionary sequence between 3.4 Ma and 0.01 Ma in the Tarim Basin were established [20]. Researchers have predicted that the area has been dominated by dry-cold stages since the Quaternary, but many short-term cold and warm alternations have also occurred in some periods. Second, by studying the grain size characteristics, sporopollen and changes in oxygen isotopes in carbonate in the Quaternary sediments in the borehole, the depositional processes in the borehole area that formed the cold-dry fluvio-lacustrine facies in the early Pleistocene to the warm-wet lacustrine facies in the low-lying land in

the early middle Pleistocene to the dry-cold aeolian facies in the late Pleistocene were revealed [21]. Moreover, the strata are further divided into three relatively warm-wet short depositional periods [22]. The results of the particle size analysis of lacustrine sediments in the LX02 profile on the north bank of the Peacock River in the northeast Tarim Basin reveal that the climate in the late Pleistocene from 72–51 ka BP changes from drought to humid to drought conditions [23,24], which are manifested as the 72.4–66.8 ka BP dry period, 66.8–56.1 ka BP warm-wet period and 56.1–51.0 ka BP dry period. Ostracod assemblage fossils indicate that a large lake surface formed in the Tarim Basin to the north of the Kuqa Depression in the Holocene [25]. Furthermore, the lithology, physical properties and pollen analysis of K1 borehole sediments in central Lop Nur in Xinjiang [26] showed that the climate fluctuated significantly in the early Pleistocene, and the climate was arid in the middle Pleistocene, as shown by the occurrence of many soft mudstone and gypsum strata [27]. The late Pleistocene pollen assemblage shows that desert and desert steppe vegetation alternated, and the characteristic pollen in the lake area in the Holocene was the desert vegetation type of pollen. The overall trend of climate change in the Lop Nur Depression in Xinjiang since the Quaternary period has fluctuated and gradually changed to drought [26,28,29]. Based on studies of lithological characteristics, thermoluminescence dating, palaeomagnetic reversal, magnetic susceptibility change and the Fe_2O_3 content in the AK1 borehole, with a depth of 465.55 m, in the Lop Nur area, a reliable Quaternary stratigraphic and age boundary since the Pliocene has been established [30]. A study of Quaternary sedimentary facies and the climatic evolutionary sequence was carried out in the Kashi Sag, northwest margin of the Tarim Basin, via 800 m-deep drilling, and the coupling relationship between climate change in this area and global glacial-interglacial climate change was obtained [31,32].

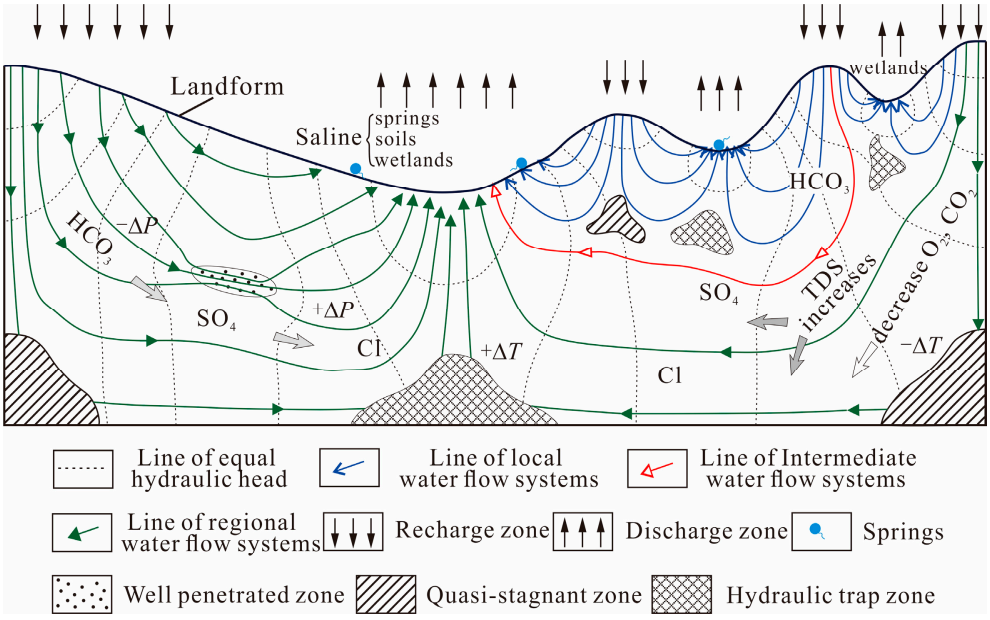

Figure 1. Evolution distribution and associated phenomena of watershed scale gravity-induced groundwater flow systems in the basin (revised by [3]).

Through detailed analysis and study of previous achievements, it is found that the research on the fundamental theories of groundwater at the scale of small and medium-sized basins in the northwest margin of the Tarim Basin is very slow, and most of the research only stays in the study of groundwater types and flow field characteristics, water resource quantity equilibrium, two-dimensional numerical simulation, short-term monitoring of water level and quality, and hydrochemical types. However, there are few studies on the mutual conversion of surface water and groundwater, the spatio-temporal distribution of stable isotopes and radioactive isotopes, and the evolution mechanism of the groundwater

flow system and its model in this basin. Meanwhile, there are still some problems to be solved: (1) to date, most of the studies have been concentrated in the eastern margin and hinterland of the Tarim Basin, but there are few comprehensive studies on the Quaternary strata in the northwest margin of the Tarim Basin; (2) there is a lack of reliable dating of Quaternary strata and key geological events; (3) regional palaeoclimate studies since the Quaternary are still lacking, especially since the last glacial period; and (4) the evolutionary pattern of GFSs since the Quaternary is still unclear. The approximate dates of the various geological events involved in the article refer to the dates published by the International Commission on Stratigraphy in five years [33]. Through detailed analysis of the hydrogeological conditions, geophysical inversions, particle size characteristics and logged stratigraphy and chronology of the Aksu River Basin at the northwest margin of the Tarim Basin, combined with the upstream glacial sedimentary sequences, pedestal terrace features and parameters from borehole KT11, which include the palaeopollen composition, magnetic susceptibility, Rb/Sr and total organic carbon, this paper restores the evolution of the sedimentary environments and palaeoclimate of this basin since the Quaternary, and then reconstructs the mechanism of the evolution of the GFS in this basin since the LGM, which enriches the study of groundwater flow theory in this distant inland ocean basin.

2. Study Area

2.1. Study Area

The mid-latitudes of the Asian continent can be divided roughly into two distinct climatic regions: a humid eastern-southern region controlled mainly by monsoon circulation (monsoon-dominated Asia) and an arid western region (including the Tarim Basin) dominated by the mid-latitude westerlies (westerly-dominated Asia) [34] (Figure 2a). The Aksu River Basin is located on the northwestern edge of the Tarim Basin, approximately 300 km from the KT11 borehole (Figure 2b). The Kumarik River and the Toxkan River are tributaries of the Aksu River, which is bounded by the southern Tianshan Mountains in the north, the Kashi Prefecture in the west, the Taklimakan Desert in the south, and Alaer city in the east. The basin is in a terrain with a gradual descent from north to south and from west to east, with distinct geomorphological zoning, and the alluvial plain is approximately 1000–1500 m above sea level. The geomorphic types of the study area are high rocky mountains (Figure 2c), intermontane basins, low rocky hills, alluvial fans, foothill alluvial fans, Quaternary alluvial plains, fine-grained soil plains and desert from the mountain to the basin center. The region is in a warm continental arid zone, with an average annual precipitation of approximately 64 mm, an annual evaporation of 1890 mm, and an average annual temperature of approximately 9.2 °C [35]. The Aksu River flows from glaciers in the central Tianshan Mountains, and groundwater generally discharges from the far north into low-lying rivers and lakes in the south, eventually entering the Tarim River through drainage networks [36]. Glaciers are present at an altitude of 3800–4800 m (the remains of glacial sediment are visible at approximately 2700 m), and its meltwater is the main water source of the Aksu River, accounting for more than 50% of the river's runoff [37]. Some watersheds have developed one- or two-foothill areas in front of the mountains that are controlled by the geological structure. Some foothills are exposed at the surface, whereas others are concealed underground.

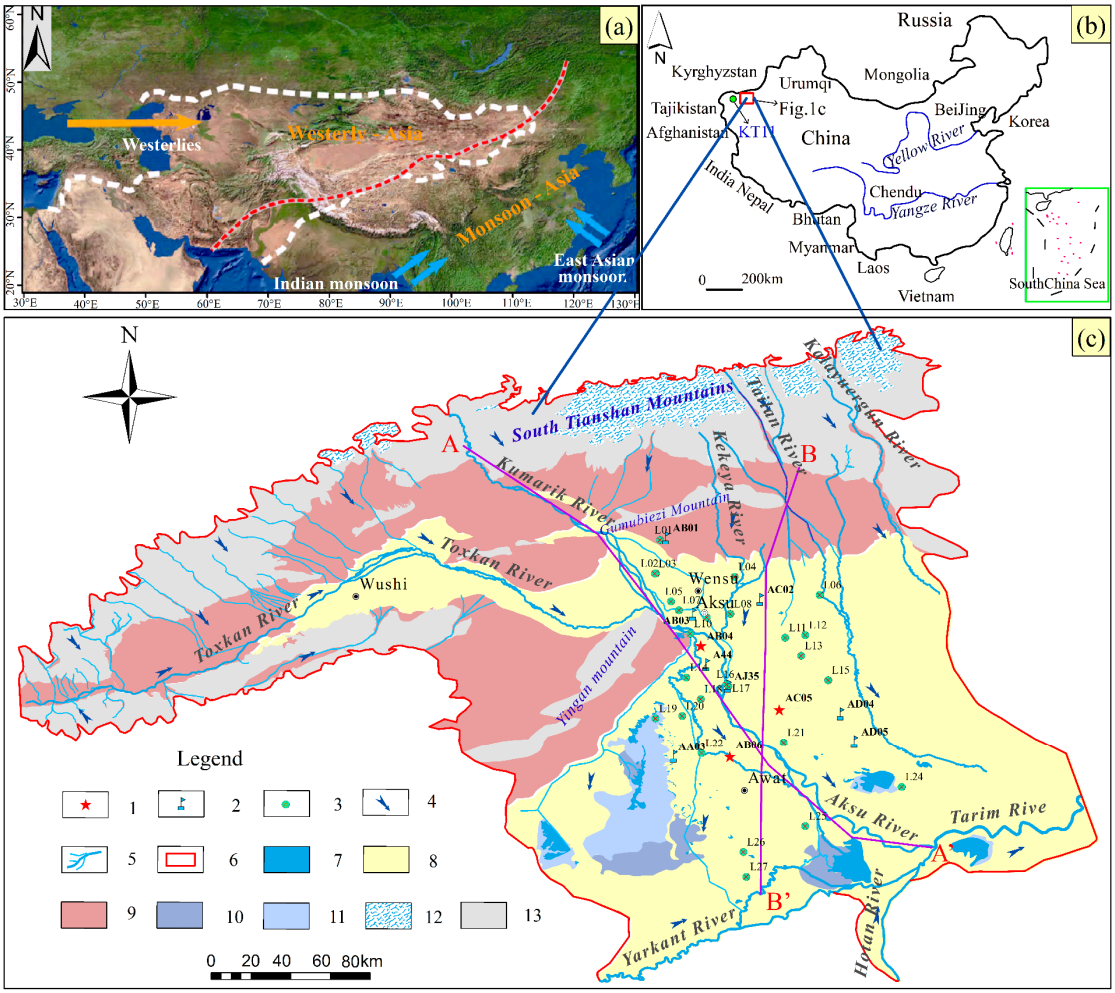

Figure 2. Division of climate control area and distribution map of geomorphology and major boreholes in Aksu River Basin. (**a**) Mid-latitude westerly wind Asia region and monsoon Asia region remote sensing image (the orange arrow labeled as 'westerlies' represents the overall direction of the wind; white dotted line: west wind Asia region, modified according to [38]; red dashed line: monsoon boundary line, monsoon Asia region, according to [39]. (**b**) Study area scope and KT11 location map. (**c**) Distribution of Quaternary sedimentary facies, river systems and major boreholes within location of the study area in the Aksu River basin (1—sample borehole, 2—reference borehole, 3—logging position, 4—groundwater flow, 5—river, 6—study area, 7—lake, 8—alluvial deposit, 9—diluvial deposit, 10—alluvial-lacustrine deposit, 11—lacustrine deposit, 12—moraine deposit, 13—bedrock outcrops, A-A′ and B-B′—hydrogeological profiles).

2.2. Hydrogeological Conditions

Based on the hydrogeological and lithological properties, the study area was divided into the northern intermontane basin (north of Tumuxiuke town), alluvial-diluvial inclined zone in front of Gumubiezi Mountain (between the Gumubiezi Mountains and Wensu County), gravel plain area (from north of the southern Aksu district to Jiamu town), and a granular plain area with fine soil (south of the southern Aksu district). The Quaternary hydrogeological units in the study area are composed of a shallow aquifer system, a middle aquifer system and a deep aquifer system (Figure 3). North of the southern Aksu district area, the aquifer system is phreatic water regardless of the depth. The shallow aquifer system corresponds to the Holocene and upper late Pleistocene strata, with a fast renewal rate and strong water enrichment. The middle aquifer system corresponds to the lower late Pleistocene stratum, with a weaker renewal rate than the shallow aquifer system. The deep aquifer system corresponds to the middle Pleistocene stratum, with a very slow

renewal rate, and the entire shallow, middle and deep aquifer system is composed of pebble gravel and sandy gravel. The material that composes the shallow, middle and deep aquifer system consists of gravel-cobbles and sandy gravel. Confined water is separated by stable aquitards. In the area south of the southern Aksu district, the correspondence between the aquifer system and the rock strata has remained unchanged, but the particle size gradually becomes finer and consists mainly of sand and clay; the type of groundwater also changes, with only the shallow aquifer system being phreatic water and the middle and deep aquifer systems being confined water. The particle size reveals a very strong spatiotemporal regularity, i.e., horizontally from north to south, with gravel, coarse sand, fine sand and clay, and vertically upwards to the alluvial plain area, demonstrating the characteristics of becoming sequentially coarser from top to bottom. Hydrogeological mapping shows that there is a hidden palaeodiluvial fan from Xidaqiao to southern Kumubashi Township, with a depth of 80 m at the top surface, and the burial depth gradually increases to approximately 200 m to the south near Kumbashi Township. The lithologies are single-lithology gravel and sandy gravel (see boreholes AB04 and 44 for details). It is speculated that this may be due to the rapid accumulation of many molasse formations at the front of the mountain during the rapid uplift of the South Tianshan Mountains, which led to the southwards extension of the diluvial fan, with abundant sediment sources [40].

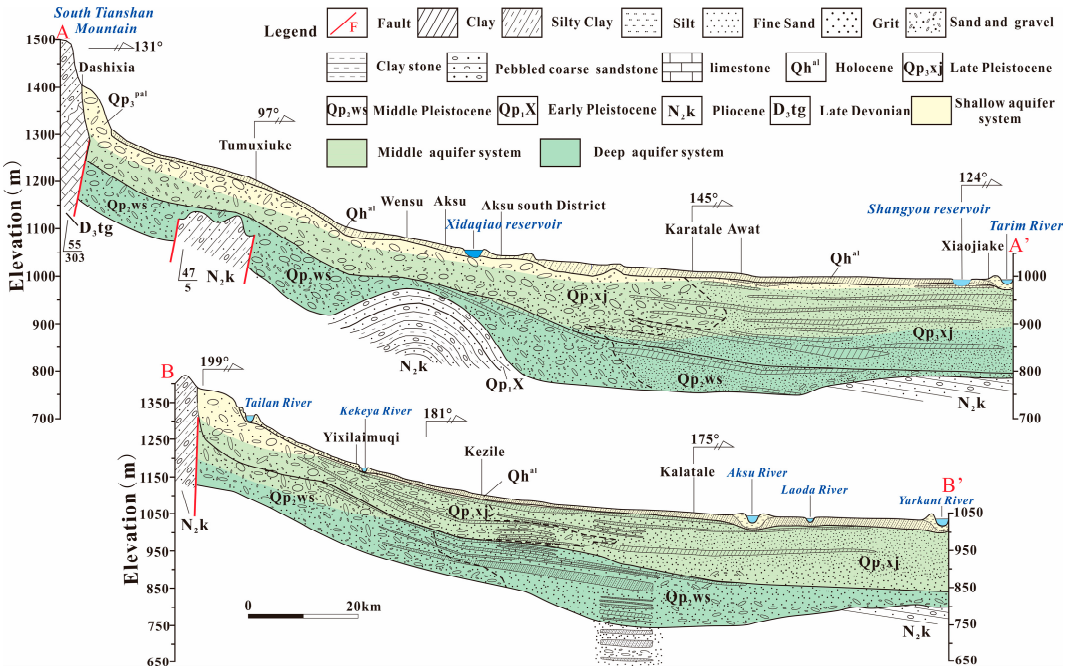

Figure 3. Comprehensive hydrogeological profile in the Aksu River Basin. (The positions of profiles A-A′ and B-B′ are shown in Figure 2c).

3. Date and Methods

In this paper, three boreholes, AB02, AB06 and AC05, with relatively complete lithofacies outcrops in the middle and lower reaches of the Aksu River, were selected as the research objects. The borehole depths were 204 m, 250 m and 402 m (Figure 4), and borehole AC05 was used only for a discussion of deep extension. All of the stratigraphic columns made from the borehole data were determined based on core samples taken during research and reference boreholes. Moreover, AB02 and AB06 were selected as the representative boreholes (the rest were the reference boreholes) to study the sedimentary palaeogeographic information that shows the response of the logging curve.

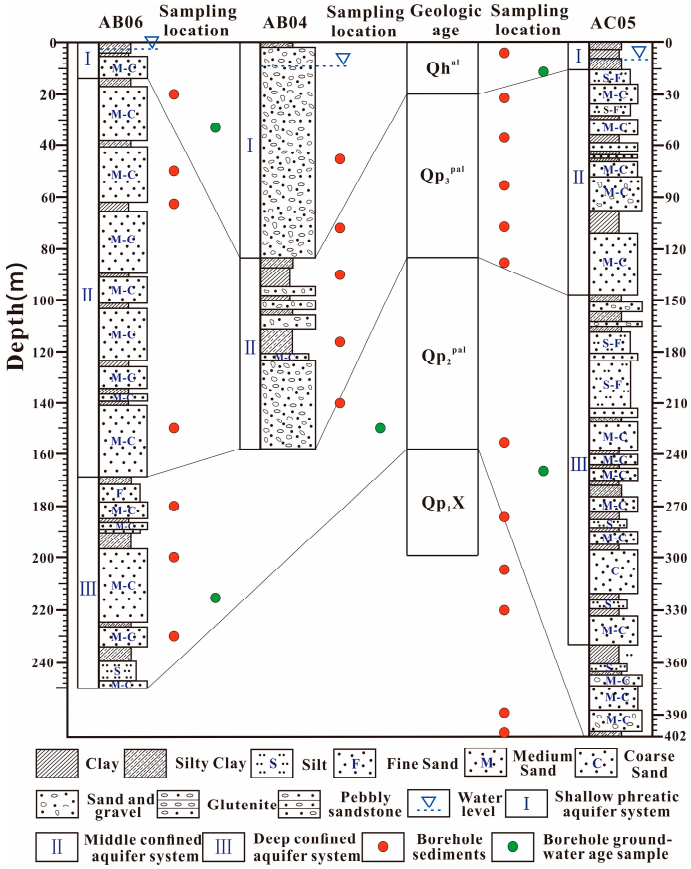

Figure 4. Distribution of lithology, aquifers and sampling locations in boreholes AB04, AB06 and AC05.

3.1. Particle Size Analysis

The sieving method and settling velocity method were used for particle analysis of 58 sediment samples (including those from reference boreholes) from the extracted borehole cores [41], which gave parameters such as the sediment lithology, particle size, particle components, average particle size and sorting. The sampling density was collected from top to bottom according to the distribution and variation in thickness of different lithologies, and the two methods were suitable for loose sediments with particle size greater than and less than 0.075 mm. The sieving method was to screen the sandy-gravely sediment in the borehole, and different sieve sizes were used (the size of the sieve used for analysis was determined based on the properties of the particles and the application requirements), separating different particle size components, weighing their respective weights and calculating the percentage of the sample mass that was less than the mass of a given particle size within the total mass, as shown by the following equations:

$$X = \frac{m_A}{m_B} \cdot x \tag{1}$$

$$C_u = \frac{d_{60}}{d_{10}} \; and \; C_c = \frac{(d_{30})^2}{d_{10} \cdot d_{60}} \tag{2}$$

where X is the percentage of the sample mass that it is less than the mass of a given particle size within the total mass (%); m_A is the sample mass that is less than some particle size (g); m_B is the mass of the sample taken for fine sieve analysis and the total mass of the sample for coarse sieve analysis (g); x is the percentage of the mass of a sample with a particle size of less than 2 mm to the total mass (%); C_u is the coefficient of nonuniformity; C_c is the

coefficient of curvature; and d_{10}, d_{30} and d_{60} are the particle sizes when the sample mass accounts for 10%, 30% and 60% of the total mass, respectively.

The settling velocity method involves adding 10 mL of $(NaPO_3)_6$ at a concentration of 4% to a certain mass of the sample, mixing it to form a 1000 mL suspension, and distributing the particles in the suspension uniformly. At this time, particles of different sizes in the suspension sink at different speeds. The diameters of the differently sized particles in the suspension were calculated according to Stokes' law (the settling velocity is proportional to the square of the diameter of the sediment), which in turn was determined by using a liquid densitometer to determine the percentage of mass of the corresponding differently sized particles [42].

3.2. Geophysical Probing Technique

Large-scale geophysical inversion work was carried out in the area south of Tumuxiuk town, and combined with the degree of cementation of rock formations and the lithofacies and chronological results from outcrops that were unearthed by drilling, the burial depths of loose sediments from the lower Pleistocene (above the basement) to the Holocene were restored. Second, geophysical logging techniques were used to measure the resistivity and self-potential of rock strata along the borehole wall; these techniques were frequently used because different physical properties show different characteristics for the transport distance and sedimentary environment of debris. A standard electrode system is used for logging, consisting of 4 electrodes. The combination method is 1 power supply electrode, 2 measuring electrodes, and the 4th electrode as a power supply electrode connected to the wellhead casing. The electrode is made of stable lead material, with a diameter of no more than 3 cm and a length of no more than 3–5 cm. In practical work, one of the paired electrodes that is far away from the non-paired electrode is usually arranged on the ground, and there is only one power supply electrode and one measurement electrode on the downhole electrode system. The potential electrode system with an electrode distance of 0.25–0.75 m is generally used in the plain area. By interpreting and identifying the amplitude, shape, smoothness, frequency of the change, trend and combined mode of logging curves of 28 boreholes in the basin (Figure 2c), the changes in the Quaternary lithologic structure, sedimentary type, aquifer system distribution, permeability and particle size sequence and sedimentary facies of strata can be inferred, and the palaeosedimentary environment can be further restored.

4. Results

4.1. Burial Depth of Quaternary Unconsolidated Sediment Derived from Geophysical Inversion

According to the physical interpretation (Figure 5), the thickness of the loose sediments increased gradually from the middle Pleistocene to modern times, but the change in the thickness and rate of increase were not uniform in different sections. Influenced by the continued uplift of the Gumubiezi and Yingan Mountains in the late Cenozoic and the intensification of the Wensu uplift since the middle Pleistocene [43–45], the increased thickness of sediments in the area from Wensu to Jiamu decreased significantly compared to its northern and southern sides, and two subsidence centers were formed, namely, the Wushi sag on the northern side and the Awati sag on the southern side [46] (Figure 5a). During the whole process of tectonic uplift, the mountainous area of Gumubiezi and the Yingan Mountains gradually decreased due to sediment accumulation and erosion, while the range of the subsidence area gradually increased, and the morphology lengthened and widened along the NE direction (Figure 5a), especially in the area from Aksu City south to Awati County. Simultaneously, under the influence of the Keping thrust belt [47], the subsidence center of the Awati sag shifted southwestward (Figure 5b,c). The sediment accumulation center underwent many surface water submersions and it contains relatively rich groundwater, forms a large-scale water storage structure and promotes the evolution of shallow, middle and deep GFS circulation patterns. The increase and decrease in the Quaternary sediment thickness, the shift in the subsidence center position and the change

in the basement morphology all evolved with the continuous deformation of the thrust nappe structure in the southern Tianshan Mountains [48]. Moreover, the neotectonic movement also directly controlled the evolution of the sedimentary environment in the piedmont basin.

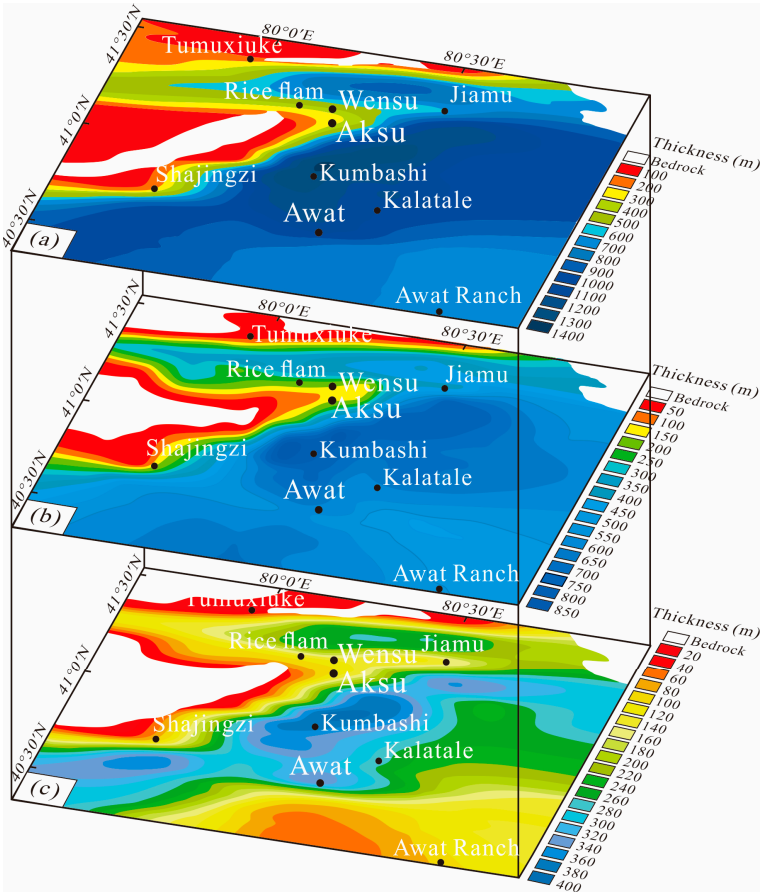

Figure 5. The evolution map of loose sediment thickness from geophysical exploration inversion since the middle Pleistocene. (**a**) modern; (**b**) the late Pleistocene period; (**c**) the middle Pleistocene period.

4.2. Glacial Sedimentary Sequence and Neotectonism

The global glacial-interglacial climatic cycle and the tectonic uplift of the mountains have left abundant glacial and aqueoglacial sedimentary sequences on the valley slopes, river valleys and foothills of the basin, which reflect cyclical glacial development and progression and extinction processes, thus directly or indirectly affecting biological evolution, climatic variations, river evolution and terrace development. The glacial sedimentary sequence from the Little Ice Age (LIA) to marine isotope stage 12 (MIS12) (Table 1) was systematically preserved and dated in the Tomur Peak area of the upper Aksu River [49]. Combined with the study of mountain glaciers in western China, it was found that the last glacial period (LGP) interglacial stage (the equivalent of MIS3b) was a cold-wet period, with abundant rainfall that led to the emergence of high lake surfaces (Great Lakes period) on the Tibetan Plateau, as well as in the Hexi Corridor and Xinjiang in inland China [50–52]. This phenomenon was also echoed in the study area [53,54], resulting in the flooding of alluvial plains and the enhancement of low-lying land and shallow lacustrine sedimentation in the Aksu River Basin during the same period, which corresponds to the lacustrine facies and fluvio-lacustrine facies in several boreholes of the same period in the study area.

Table 1. Glacial sedimentary sequence (GSS) from LIA to MIS12 and its optically stimulated luminescence (OSL) and electron spin resonance (ESR) dating data in Tomur Peak area, upper Aksu River.

IDX	Tomur River		Tailan River		Ateaoyinake River		Muzhaerte River		Events
	Stage (ka BP)	GSS	Stage (ka BP)	GSS	Stage (ka BP)	GSS	Stage (ka BP)	GSS	
1	1.35–1.8	I	1.5–1.6	I			1.6–1.7	I	LIA
2	<8	II	6.3	II	7.3 ± 0.8 (OSL)	I		II	NG
3			12.4, 13.0	III (Inside)	12.3 ± 1.2 (OSL)	II (Inside)			YD
4	20.1 ± 1.5, 18.7 ± 1.3, 20.8 ± 1.7	III	16.2, 4.1, 6.9, 16.8, 17.7, 21.7	III (Outside)	15.0, 18.3, 21.5, 27.2, 28.7	II (Outside)	13.6, 24.5, 25.3	III (Band One)	LGM (MIS2)
5					46.5 ± 4.7, 51.3 ± 5.1, 54.4 ± 5.4	III	39.5, 40.4	III (Band two)	MIS3b
6					56.1 ± 5.6, 64.4 ± 6.4	IV	64.2, 71.7	III (Band three)	MIS4
7	134.4 ± 13	IV	143.6, 147.6	IV	155.8 ± 15.6, 234.8 ± 23.5	V	208.1	IV	MIS6
8	418.9 ± 40 440.6 ± 42	V		V	453 ± 45.3	VI			MIS12

Note: I, II, etc. represent the first and second sets of glacial sedimentary sequences; OSL and ESR dating data were obtained from [53,55]; NG and YD are short for Neoglaciation and Younger Dryas, respectively; MIS3 et al. stands for deep-sea oxygen isotope stage 3.

Based on the comprehensive analysis of the tectonic history and sedimentary characteristics of the riverbed at the outlet of the Kumarik River in the foothills, as well as the palaeo-riverway elevation data, karst landform development and the characteristics of terrace exposure on both sides of the valley revealed by nearby boreholes, the vertical evolutionary pattern of the Kumarik River valley is revealed; that is, it has experienced four stable periods and three erosive periods since the Quaternary [56] (Table 2), which has led to the formation of terraces I–IV (all rock-seated terraces). Moreover, the continuous leftward deviation of the river valley was found as the valley was eroded. Using thermoluminescence dating data of the terraces, the erosion rate of the river valley was calculated, indicating that the valley's erosion rate has peaked at 8.2 m/ka from 70–80 ka BP since the late Pleistocene, and such an extremely rapid and prolonged tectonic uplift favors the possibility of a large-scale forward extensional accumulation of palaeodiluvial fans in the runoff direction during the 60–80 ka BP stable erosive period.

Table 2. The valley variation characteristics since the Epipleistocene in the upper reaches of the Aksu River.

IDX	Stage (ka BP)	Stable-Erosive Cycles	Sediment-Erosive Rate (m/ka)	Terraces
1	10–20	Stable period	0.7	I
2	20–30	Erosive period (submaximum)	3.3	II
3	30–40	Stable period	0.6	
4	40–60	Erosive period	1	III
5	60–70	Stable period	0.8	
6	70–80	Erosive period (maximum)	8.2	IV
7	80–100	Stable period	1.3	

4.3. Sedimentary Facies in Quaternary Aquifer Systems

Each sedimentary facies has its own characteristics, such as the lithology, coarse grain size, sorting, cement type, trace fossil content and sedimentary structures, as well as different physical property parameters.

4.3.1. Parameters Determined by Particle Size Analysis

Grain size analysis parameters are an essential basis for identifying sediment types and judging the formation conditions, hydrodynamic strength and sedimentary environment of sediments [57]. The C_u is generally greater than 1, and the closer it is to 1, the better the particle sorting. The C_u values of different rock layers in the study area generally show a pattern of gravel layer > clay and silt layer > sand layer. The Aksu River Basin has typical premountain alluvial-diluvial accumulation landforms, and they mainly include fluvial facies, diluvial fan facies, lacustrine facies and fluvial-lacustrine facies [40]. The fluvial sediments in the upper reaches are coarser than those in the middle and lower reaches. The Kumarik River-Toxkan River alluvial plain belt and the Xidaqiao-Yingan Mountain foothills are dominated by pebbles. The gravel diameters are mostly approximately 3–5 cm, the sorting and rounding are much better than those of the diluvial gravel, and the gravel composition includes granite, red sandstone, etc. (from Tianshan) that are not found in diluvial gravel. The alluvial plain zone surrounding the middle Aksu River near Xidaqiao is dominated by light yellow and yellow-brown coarse sand and gravel, primarily with gravel diameters of 2–3 cm; the compositions are granite, limestone, sandstone and metamorphic sandstone, etc.; the sorting and roundness are good, and the bedding is clearly defined. The grain size of the downstream particles gradually fines to the south, and its rock assemblage mainly evolves into medium-fine sand, with light yellow sandy clay and oblique bedding. The average particle size and C_u values of the middle and upper stream particles are large (smaller than the diluvium), with smaller C_c values, and more than 90% of the fractions have particle sizes larger than 100 μm, which are mostly in the upper-fine and lower-coarse binary structure; however, they generally decrease downstream.

Diluvial fan facies are generally composed of gravel and sandy gravel, sandwiched between fine sand and sandy clay layers, with sizeable average grain sizes and C_u values, small C_c values and more than 90% of fractions with grain sizes larger than 100 μm, which are dominated by jumping and rolling transport, indicative of high-energy hydrodynamic environments. Lacustrine facies sediments are generally composed of grey clay and silt, sandwiched between multiple layers of cyan grey, grey–white fine sand and silty sand, with a smaller average particle size and C_u than the other facies, larger C_c than the other facies, and almost 100% of the components with particle sizes less than 100 μm, which is indicative of weaker and more stable hydrodynamic conditions and predominantly suspension transport. The fluvial-lacustrine facies have the characteristics of both lake and river depositional phases; the average grain size and inhomogeneity coefficient are between the two values, and the fine and coarse particles are mostly interbedded and uneven, indicating that there were two or more kinds of sedimentation involved, reflecting the complexity of the depositional environment.

4.3.2. Electrofacies Analysis

Core samples are often limited, so it has become common to study the lithologic change, sedimentary rhythms and spatial distribution of sedimentary facies by using the theory of logging stratigraphy. Based on studies of the borehole lithology, lithoelectric relations, and sedimentary rhythms and cycles, combined with factors such as the logging curve shape, amplitude, contact relationship, smoothness and combined shape (Table 3), the electrofacies pattern of the study area was established by repeatedly comparing and analyzing the logging curve characteristics of the known typical sedimentary facies in the reference hole (Figure 6).

Table 3. Quaternary logging curves and main lithology characteristics in the Aksu River basin.

Parameter	Gravel-Cobble or Gravel	Sand Gravel	Sand	Clay
Size	Vary greatly, more than 2 mm	Vary greatly, 0.25–2 mm or more	Coarse sand 1–2 mm, medium sand 0.5–1 mm, fine sand 0.2–0.5 mm	Less than 0.05 mm, powder form
Rounding and sorting	General, local better	Middle	well	
Sedimentary environment	Diluvial fan, palaeochannel, moraine, etc.	Alluvial–diluvial fan, palaeochannel, etc.	palaeochannel, floodplains, oxbow lakes, etc.	Alluvial plains, lakes, etc.
RT	Vary greatly, 30–100 Ω.m	Vary greatly, 30–100 Ω.m	10–50 Ω.m	10–30 Ω.m
SP	General negative anomaly	General negative anomaly	Generally negative anomaly, occasionally positive anomaly	Very little change
Porosity	30%	30%	40%	50%
Hydraulic conductivity	25 $m \cdot d^{-1}$–42 $m \cdot d^{-1}$	25 $m \cdot d^{-1}$–30 $m \cdot d^{-1}$	2 $m \cdot d^{-1}$–25 $m \cdot d^{-1}$	Aquitard
Curve shape	Medium to high anomaly amplitude, funnel shape or box shape	Medium to high anomaly amplitude, box or bell shaped	Abnormal obvious, regular, bell, finger and tooth shape	Medium amplitude, low RT value, mostly left convex shape

Note: The hydraulic conductivity is derived from [58]; RT and SP represent resistivity and self-potential, respectively.

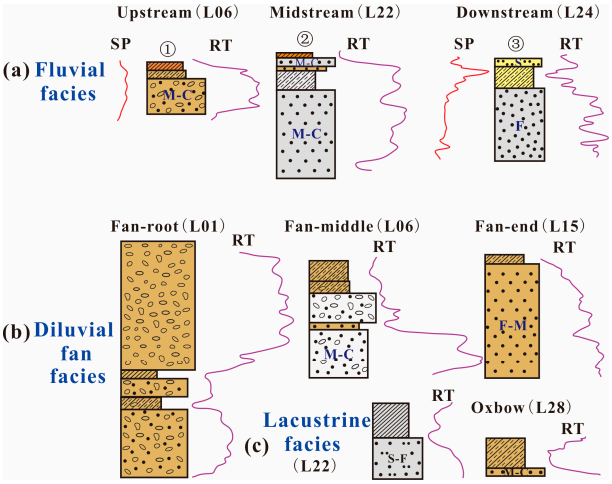

Figure 6. Identification and establishment of electrofacies pattern in the study area ((**a**)-fluvial electrofacies pattern, among them, ①, ②, ③ represent the upper, middle and lower reaches of the river facies respectively; (**b**)-diluvial electrofacies pattern; (**c**)-lacustrine electrofacies pattern). The lithology legend refers to Figure 3, where the yellow series represents that the lithology color is light yellow, tan and brick red, and the gray series represents light gray, off-white and gray.

At different stages of river evolution, the resulting rhythm of the superposition of the rock assemblage is different, so the logging curve characteristics are also different. In the upper reaches of the river, the upper part of the rock assemblage is mostly thinly layered sandy clay with horizontal stratification and a positive grain sequence in the bedding, with occasional fine sandy interlayers; the lower part is thickly layered gravel with better rounding than the grains in the upper part, and the logging curve is a box shape with a medium amplitude [59], reflecting either the hydrodynamic stability during the sedimentation process or a sufficient and diversified material supply, which accumulated rapidly (Figure 6a①); the upper part of the lithology in the midstream area is mainly sandy clay that is loose and contains small holes, and it is occasionally interlayered with silty sand or fine sand; the lower part is mostly rounded gravel that is mainly the result of meandering river deposition, and the resistivity curve is mostly box- or finger-shaped (Figure 6a②), reflecting a trend of the gradual weakening of hydrodynamic forces from bottom to top in the sedimentation process. Compared with the middle part of the stream, the upper part of the downstream rock assemblage has remained unchanged, while the lower rock assemblage gradually changes to medium-coarse sand and fine sand; the rhythmic pattern

is superimposed due to the lateral erosion of the meandering river, so the logging curve is mostly bell-shaped or tooth-shaped (Figure 6a③), reflecting frequent energy changes in the sedimentation process.

The diluvial fan facies mostly developed in the intermontane basin and alluvial-diluvial inclined zone in front of the Gumubiezi mountains and extended to its farthest depositional position in the late Pleistocene (buried palaeodiluvial fan near Xidaqiao). The electrofacies pattern of the diluvial fan, including the three microfacies of the fan root, fan middle and fan end, was established (Figure 6b); these microfacies are generally funnel-shaped, bell-shaped and tooth-shaped, respectively, and more often have curved jagged residual layers (caused by poor roundness). The lacustrine facies developed only in the downstream low-lying areas, and the lithology is clay and silt, with visible laminae; the facies yielded straight-shaped self-potential and a left convex-shaped resistivity curve (Figure 6c), reflecting weak and stable hydrodynamics.

4.3.3. Sedimentary Facies Division

The evolutionary stages of the sedimentary environment since the late Pleistocene were obtained through a comprehensive analysis of the lithologic characteristics, main grain components, sorting, rounding and logging curves of the sediments from boreholes AB04 and AB06, and reference boreholes (Table 4).

Table 4. Particle characteristics and sedimentary facies division of boreholes AB04 and AB06.

IDX	Sedimentary		Major LC	PS Range (Avg.) μm	C_u	RT Curve Shape	Sedimentary Faces	Sedimentary Microfacies
AB04	I (0–100 m)	0–83 m	sand + gravel (>95%)	442–468 (455)	5–22 (14)	box, finger shape	fluvial faces	riverbed
		83–100 m	silt + sand (90%)	6–496 (129)	5–14 (8)			flood plain
	II (100–111 m)		sand + gravel (80%)	9–496 (334)	7–21 (16)	tooth shape	diluvial fan facies	fan-root
	III (111–123 m)		silt + sand (93%)	9–340 (174)	2–7 (4)	left convex shape	fluvio-lacustrine facies	low-lying land
	IV (123–150 m)		sand + gravel (>95%)	496–577 (536)	20–22 (21)	funnel shape	diluvial fan facies	fan-root
AB06	I (0–14 m)		silt + sand (>95%)	5–268 (94)	2–15 (9)		fluvio-lacustrine facies	
	II (14–123 m)		silt + sand (>95%)	6–268 (149)	8–15 (6)	bell shape	fluvial faces	riverbed or flood plain
	III (123–125.4 m)		clay + silt (>95%)	5–6 (5.5)	6–10 (8)	left convex shape	lacustrine facies	low-lying land
	IV (125.4–168.1 m)		silt + sand (>95%)	6–268 (163)	2–8 (4.8)	box shape	fluvial faces	
	V (168.1–188.6 m)		silt + sand (91%)	6–268 (129)	2–15 (6.5)	tooth shape	fluvio-lacustrine facies	
	VI (188.6–196.1 m)		clay + silt (>95%)	8–94 (51)	4–15 (9.6)	left convex shape	lacustrine facies	shallow lake
	VII (196.1–234.1 m)		silt + sand (93%)	8–268 (181)	2–15 (6.6)	box shape	fluvial faces	flood plain
	VIII (234.1–250.2 m)		silt + sand (89%)	8–268 (123)	2–15 (7.3)	tooth shape	fluvio-lacustrine facies	

Note: Lithological components and particle size are abbreviated as LC and PS, respectively. RT represents resistivity.

The Quaternary-confined aquifer system of the Aksu River watershed began to evolve in the midstream and downstream alluvial plain areas, and its process was obviously related to the Quaternary sedimentary cycle and is basically consistent with the distribution of sedimentary facies. Although the bottom of borehole AB04 has not been investigated, the confined aquifer system is present, and it is composed of middle Pleistocene and early late Pleistocene (Qp_2ws-Qp_3xj) strata [53,56,60]; the sedimentary lithofacies changes from diluvial fan facies composed of sandy gravel at the bottom to fluvial–lacustrine transitional facies composed of medium sand and silty clay at the top (Figure 7a), the average particle size and C_u decrease from 536 μm and 21 to 174 μm and 4, and the logging curve changes

from funnel-shaped to left-sided convex-shaped. The shallow phreatic aquifer system is mainly composed of late Pleistocene (Qp_3xj) and Holocene (Qh) strata, and the sedimentary lithofacies from bottom to top mainly consist of diluvial fan facies composed of poorly sorted and rounded sandy gravel with silty clay interlayers and fluvial facies composed of better-sorted and rounded gravel and silty clay. The average particle size and C_u decrease from 334 μm and 16 to 455 μm and 14, respectively, and the logging curve changes from tooth-shaped to box- or finger-shaped. The sedimentary facies division of borehole AB06 is shown in Figure 7b, and the largest difference from borehole AB04 is that AB06 is located downstream of the river, and the C_u value of the silty clay layer is higher than that of the fine sand and medium sand layers, which causes its curve to display the opposite characteristic to that of the average particle curve.

An analysis of the evolutionary pattern of the sedimentary environment of the whole Quaternary aquifer system reveals that the evolution of the sedimentary environment was controlled by the tectonic uplift and subsidence of the topography of the basin basement, the change in the hydrodynamic strength driven by the water potential difference caused by the melting of glaciers in the upstream regions (i.e., the transport capacity of the river) and other conditions. Since the LGM, the Aksu River Basin has mainly been dominated by a deep-cutting palaeochannel and the continuous iteration of the palaeoalluvial plain, which has influenced and transformed the evolutionary model of the basin's sedimentary environment.

4.4. Characterization of the Palaeoclimatic Evolution

A comprehensive study of the palaeoclimatic evolution since the Quaternary at the northwest margin of the Tarim Basin was carried out by combining lithology, palaeomagnetism, sporopollen and other data, revealing the palaeoclimatic evolutionary sequence.

4.4.1. Quaternary Palaeoclimatic Evolutionary Sequence

The latest, most detailed and complete research results on the palaeoclimatic evolution in the study area come from Quaternary borehole KT11 in the Kashi depression area, northwest margin of the Tarim Basin (Figures 2b and 8), indicating that it is basically consistent with the evolution of the palaeoclimate in the hinterland and northeast margin of the Tarim Basin [32]. Overall, dry-cold climates have characteristics of high total organic carbon, finer grain size, lower magnetic susceptibility [61] and higher Rb/Sr values [62], as well as the vegetation type of steppe or sparse forest grassland (obtained by the analysis of sporopollen assemblage), whereas warm-humid climates have characteristics of low total organic carbon, coarser grain size, higher magnetic susceptibility, lower Rb/Sr values and vegetation types of coniferous broad-leaved mingled forest and grassland [63]. According to the results of previous studies, the climate change around the Tarim Basin since the Quaternary has similar spatiotemporal evolutionary characteristics, which can be divided into four stages. In the early Pleistocene, the climate in the hinterland and northwest margin of the Tarim Basin was mainly cold-dry, but in the northeast margin of the Tarim Basin, the climate alternated between dry-cold and warm-wet [27]; in the middle Pleistocene, the hinterland and northwest margin of the Tarim Basin were characterized by warm and humid climates, while the northeast margin contained a warm-wet climate mixed with a short dry-cold climate. From the late Pleistocene to the Holocene, the whole Tarim Basin entered a long-term dry-cold stage, whereas the Holocene was dominated by a warm-arid climate [30,39].

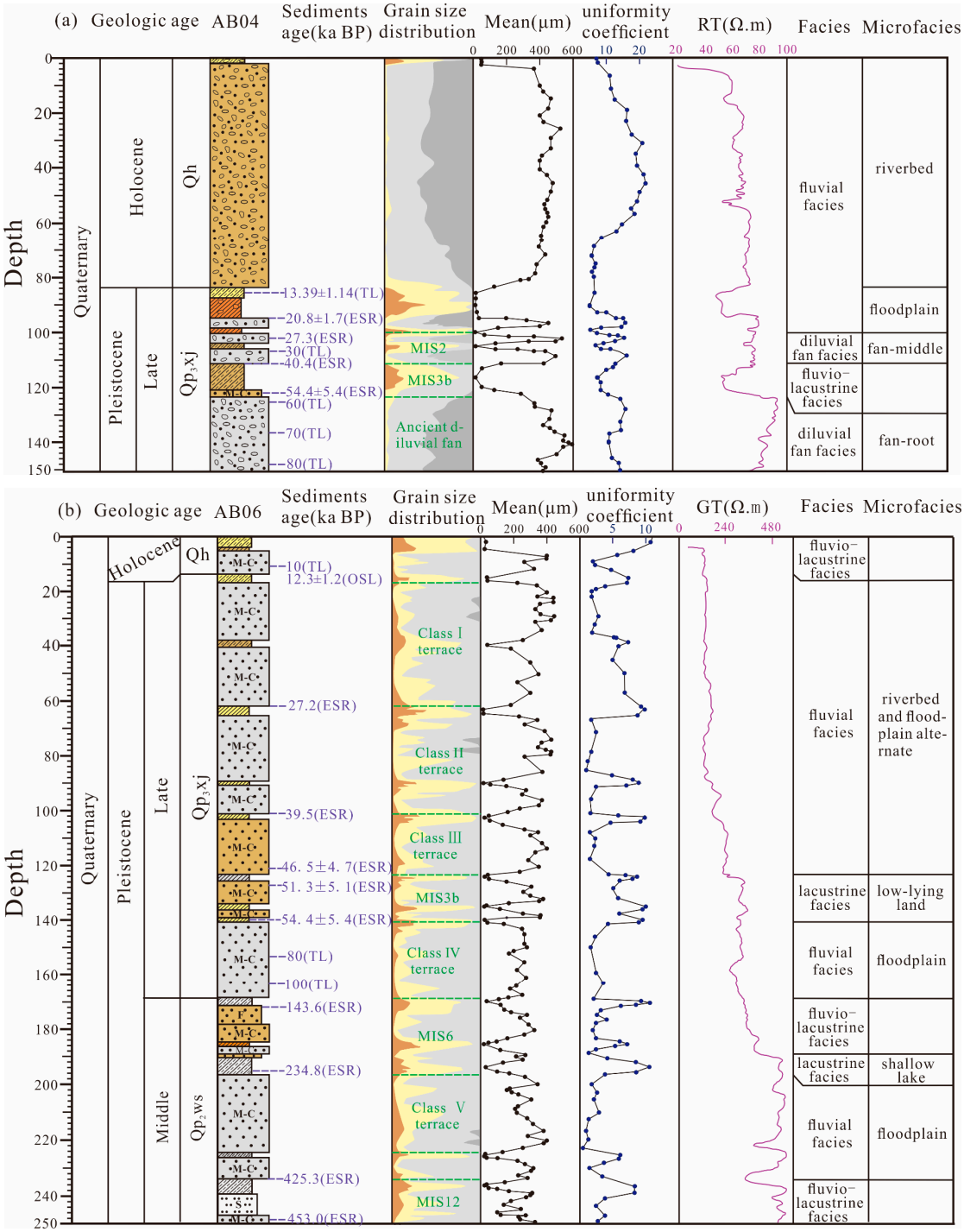

Figure 7. Lithological combination characteristics, particle size distribution, log facies and categorization of sedimentary facies in boreholes (**a**) AB04 and (**b**) AB06. The thermoluminescence (TL), electron spin resonance (ESR) and optically stimulated luminescence (OSL) ages of boreholes AB04 and AB06 were obtained from [49,53], respectively; the fluvio-lacustrine sedimentary facies were formed by the combination of fluvial sedimentary facies, lacustrine sedimentary facies or transitional sedimentary facies; refer to Figure 5 for lithology legend in this figure; in the grain size distribution, brown is clay, light yellow is silt, light gray is sand, dark gray is gravel and the green letters correspond to typical landforms and ice ages.

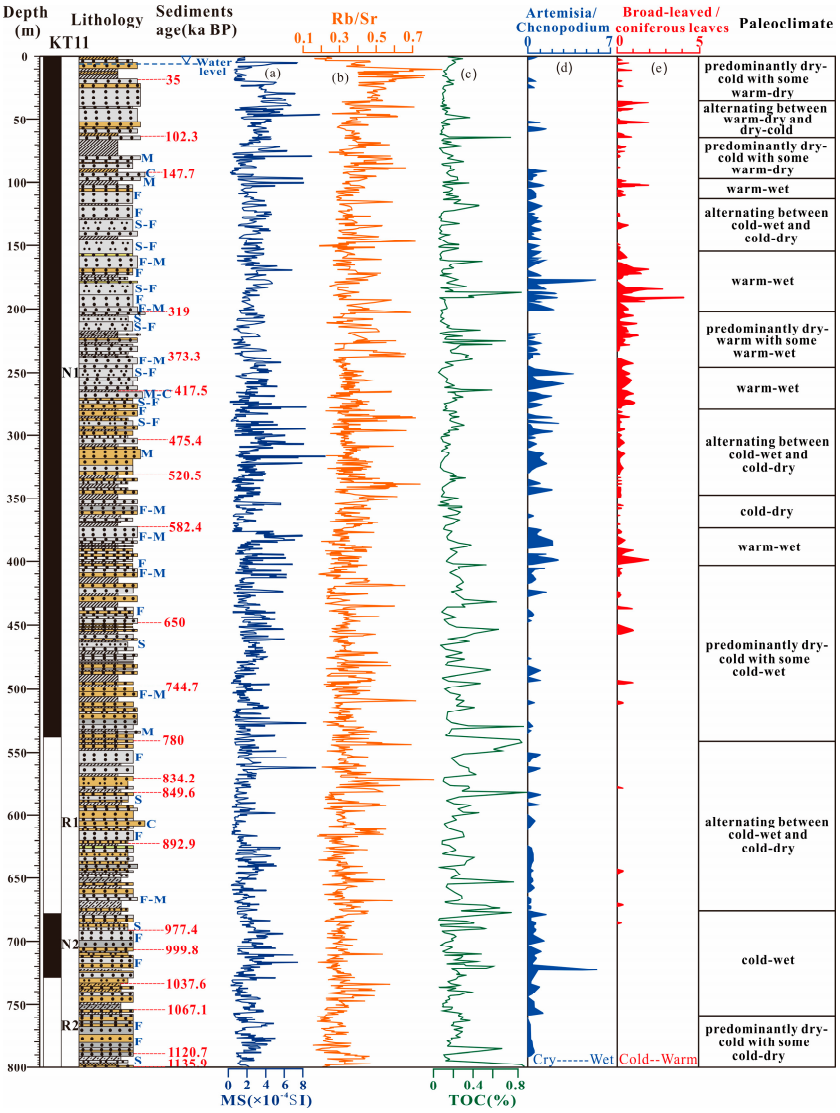

Figure 8. Lithological combination characteristics, magnetic susceptibility (MS) (**a**), Rb/Sr (**b**), total organic carbon (TOC) (**c**) and sporopollen assemblage (**d**,**e**) of borehole KT11, with its paleomagnetic age [32,33,64]. The lithology legend refers to Figures 3 and 5.

The correspondence between climate change and sedimentary environments was investigated in the fluvial-lacustrine sediments of borehole KT11 using optically stimulated luminescence dating and gamma-ray logging (reflecting the relative abundance of clays and sands) techniques. Simultaneously, these results were compared the $\delta^{18}O$ values of the Guliya ice core from the Tibetan Plateau, the $\delta^{18}O$ values of the Greenland ice core, the Chinese Loess Plateau grain size record from Gulang and the climate change characteristics reflected by the MIS4, MIS3 and MIS2 stages, reflected by deep-sea oxygen isotopes (Figure 9); and finally, a reliable high-resolution climate chronology was established for the northwest margin of the Tarim Basin since the LGP [33]. Climate change shows regional development. Gamma-ray and average grain size data from the KT11 borehole indicate the significant influence of temperature and the water cycle on the climate in the northwest margin of the Tarim Basin. Moreover, its fluvio-lacustrine strata also seem to record Heinrich's 6 Cold Events, a Younger Dryas (YD) event, and Dansgaard-Oeschger cycles of the LGP [65,66], further reflecting that the rapid and frequent climate change in the North Atlantic had a strong controlling effect on the region, thus revealing the coupling relationship between the inland arid region of central Asia and the Atlantic westerlies [67–69] (Figure 2a). The occurrence of these events corresponds to most of the

climate events from the LIA to MIS12 that are preserved in the typical glacial sedimentary sequence in the Tomur Peak region of the upper Aksu River, thereby confirming its rationality [49,55,70].

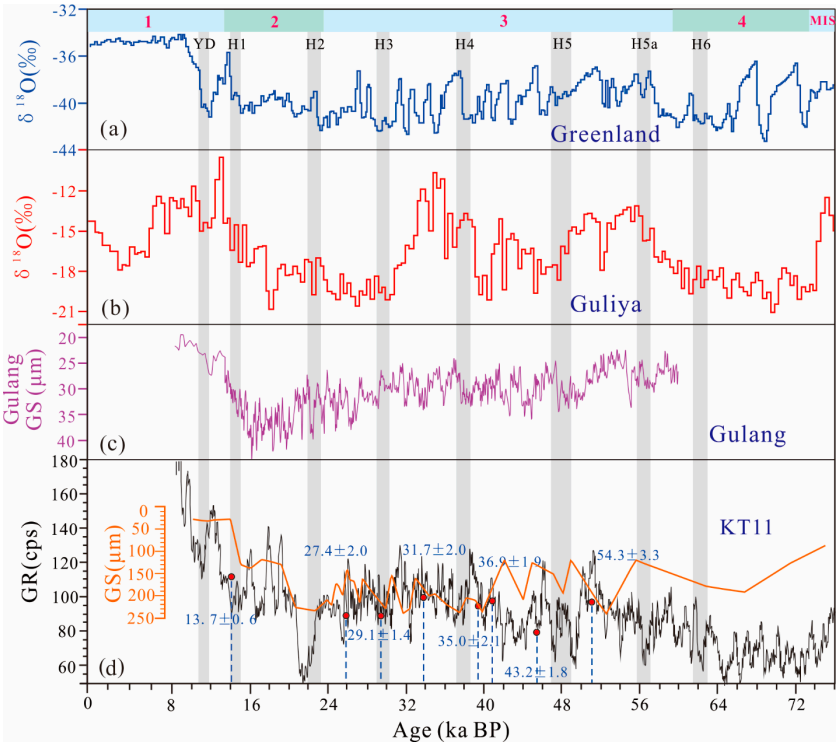

Figure 9. Climate change for the LGP at the northwestern margin of the Tarim Basin. (**a**) The distribution curve of North Greenland Ice Core Project (NGRIP) $\delta^{18}O$ records was taken from the Greenland ice cores, 2004 [71]; (**b**) The Guliya ice core records are from [72]; (**c**) The distribution curve of Gulang loess mean grain size (GS) is taken from [73]; (**d**) Gamma-ray (GR) data and GS of the KT11 borehole are from [33]. H1 to H6 represent positions of Heinrich events [66], the light blue and green color bars represent the odd and even marine isotope stages (MIS), respectively.

Through a comparative study of the combined lithology, sporopollen assemblage, particle size and age of each stage recorded in boreholes AB04 and AB06 in the Aksu River Basin and borehole KT11, and accounting for the coupling effect of climate change between the northwestern edge of the Tarim Basin and the North Atlantic Ocean (i.e., the "westerly wind modes" [74]), the timeframes for the transitional stages of climate change since the LGP were precisely matched to the same epoch in the study area to divide the palaeoclimatic evolutionary stages (Table 5).

Table 5. The stages of Quaternary paleoclimate evolution in boreholes AB04 and AB06.

Boreholes	Evolution Stages	Depth (m)	Interval Ages (ka BP)	Climate Change
AB04	I	0–83.5	0–13	warm-dry
	II	83.5–100.2	13–27	cold-dry
	III	100.2–111.2	27–40	warm-wet
	IV	111.2–123.2	40–60	cold-wet
	V	123.2–150.6	60–80	warm-wet
AB06	I	0–13.8	0–10	warm-dry
	II	13.8–101	10–27	cold-dry
	III	101–123	27–40	warm-wet
	IV	123–139	40–60	cold-wet
	V	139–168.1	60–100	warm-wet
	VI	168.1–196.1	100–235	cold-wet
	VII	196.1–250.2	235–450	warm-wet

4.4.2. Climate Change since the LGM

The LGM (an interval with a range of 26.5 to 19.0 ka BP) was the coldest period of the LGP [75–77], corresponding to the deep-sea oxygen isotope MIS2 stage. To compensate for the errors caused by incomplete sediment outcropping or rough stratigraphic division in the study area and to better reflect the detailed climate change characteristics since the LGM, combined with the climate change since 12 ka BP in the Tarim River basin [78,79] and the results of the lake evolution and climate hydrology in the arid areas of Xinjiang [80,81], and the parameters in the borehole KT11 [82], we further subdivided the four evolutionary stages since 2.7 ka BP (see Table 6 for details); these results indicated the gradual aridification of the climate since the LGM in the study area [83,84], which provides effective evidence for a comprehensive and complete explanation of the controlling effect of palaeoclimate on the deep-cutting erosion of palaeochannels, the continuous iteration of alluvial plains, the formation of aquitards and the evolution of groundwater flow patterns in the study area.

Table 6. The paleoclimate evolution stage in the study area since the LGM.

Evolution Stages	Height of the Lake Surface	Sporo Pollen Assemblage	Particle Size	Interval Ages (ka BP)	Climate Change
I	low	Ephedra, Artemisia, Chenopodium mainly	decrease	0–0.3	warm-dry
II	high	Chenopodium, Artemisia, Ephedra, Gramineae mainly	increase	0.3–0.8	warmer-drier
III	low	Chenopodium and Artemisia mainly	decrease	0.8–1.3	warm-dry
IV		Artemisia, Chenopodium mainly	increase	1.3–2.7	cold-dry

4.5. The Existing Age of Groundwater in the Aksu River Basin

The existing pattern of the GFS in the catchment is the outcome of the overlapping and nesting of groundwater flow in different evolutionary periods under the action of various factors. The distribution of the groundwater age is unconformable, and the GFS at different levels displays obvious spatial differences, with large differences in the periods of groundwater recharge. According to the distribution of the groundwater age in the Aksu River Basin [85] (Figure 10f), the hydrogeology of the intermontane basin and the alluvial-diluvial inclined zone in front of the Gumubiezi mountains (the area from Wensu north to Jiamu) mainly consists of shallow and middle aquifer systems, whereas the deep aquifer system is only slightly visible near the basement; the groundwater is basically modern water (<65 a) with a fast renewal rate, and it is circulated down to the active region at the top of the basement of the quaternary aquifer system. In the alluvial plain region to the south of Aksu city, only the shallow aquifer system is modern water (not more than 100 years), and the groundwater ages of the middle aquifer system generally vary from <1 ka to <10 ka, while the groundwater age of the deep aquifer system is even more than 10 ka. Furthermore, the palaeogroundwater age of the late middle Pleistocene strata in the Quaternary basin measured at present is up to 23.5 ka, but whether there is a superdeep GFS in the strata that predates the late middle Pleistocene is not discussed due to limited data. Therefore, the evolutionary process of the existing GFS pattern in the Aksu River Basin since the LGM can be reasonably inferred from the above analysis.

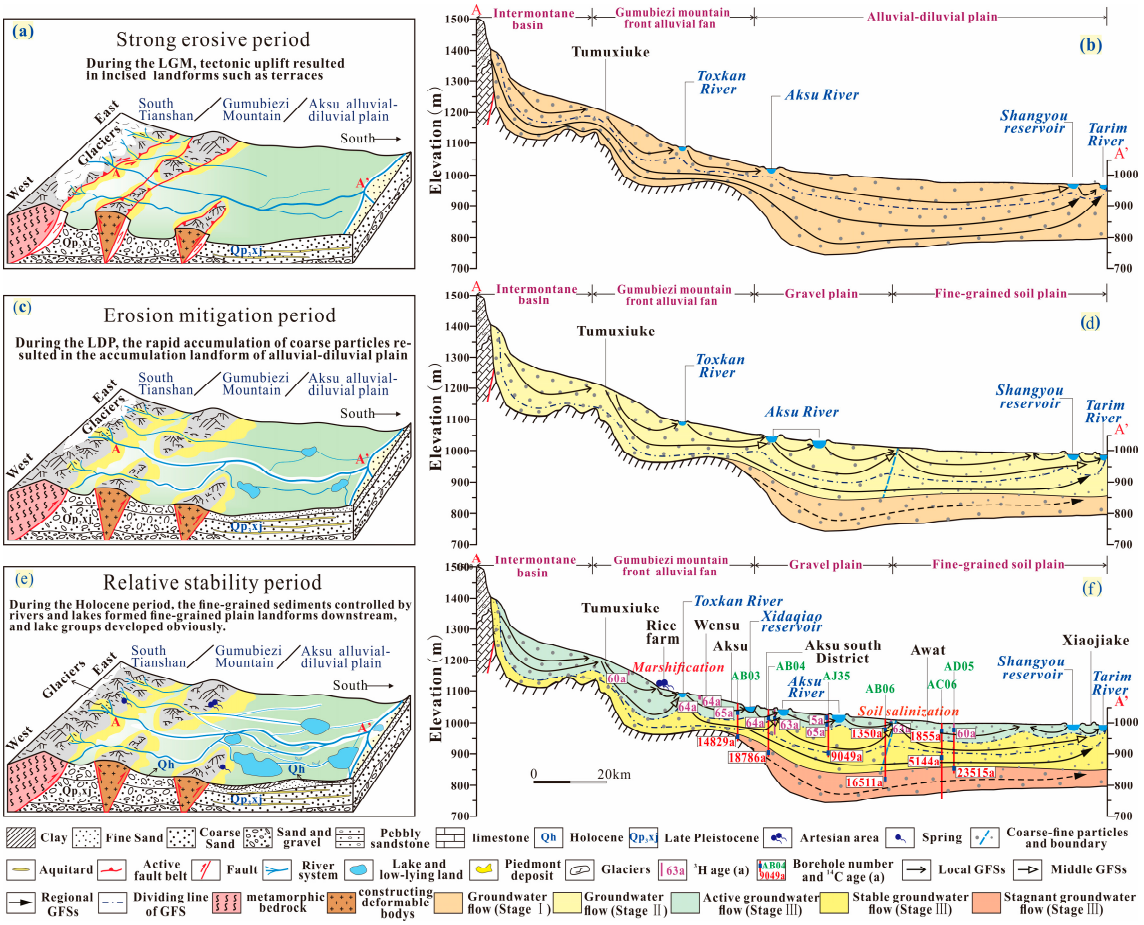

Figure 10. Schematic diagram of evolution pattern for the sedimentary environment (**a**,**c**,**e**) and the GFS (**b**,**d**,**f**) under the control of tectonic activity since the LGM in the Aksu basin. The relative age of groundwater along and near the A-A′ profile is based on [85].

5. Discussion

5.1. The Sedimentary Environment Evolution Characteristics of the Aquifer System

Thin-skinned nappe structures have frequently formed in the southern Tianshan Mountains since the Quaternary [48,86] and have remained active until the late Pleistocene [87–89]. Neotectonically, they mostly formed by sinistral and overthrust deformation, resulting in the overall uplift of the northern mountains and valleys along the river system; the river system upstream of the Aksu River gradually shifted to the left after exiting the mountain, and the GFS was readjusted. Moreover, the river carried the debris from the mountain to the front of the mountain and deposited it in the Awati fault depression, gradually forming the alluvial-diluvial plain of the Aksu River and the Kekeya River. The analysis of the sedimentary environmental evolution of the Quaternary aquifer system in the Aksu River Basin revealed that the medium- and deep-grained aquifer systems were vertically dominated by medium- and coarse-grained aquifer media, which were gradually separated until a continuous aquitard was formed in the alluvial plain area to the south of Aksu city. The sediments of the middle-deep aquifer system demonstrated a transition from diluvium to alluvium upstream of the river and the development of alluvium and alluvial and lacustrine deposits downstream; however, the particle size was generally coarser at the bottom than the top, indicating that the hydrodynamic conditions gradually weakened and became stable. By comparison, the shallow aquifer system developed mixed diluvium-alluvium in the intermontane basin and alluvial-diluvial inclined zone in front of the Gumubiezi Mountains, and the hinterland of the downstream alluvium plain was composed of weakly permeable alluvium and lacustrine fine-grained layers, indicating that the

hydrodynamic conditions were further horizontally weakened. There is a certain coupling relationship between sedimentary facies cycles and climate change [90], which has been fully reflected in the sedimentary environment evolution of the Aksu River Basin since the LGM. This evolutionary process is also closely related to glacier advance and retreat in the Tomur Peak area and tectonic uplift, and it can be divided into three evolutionary stages.

Stage I (cold-dry climate period): During the LGM, the climate was the coldest and driest, with low surface temperatures. Due to tectonic uplift and dramatic river level decline, the local erosional base level of the Aksu River Basin was kept at an extremely low level, which led to the strong downcutting of the river in the study area, resulting in the formation of geomorphological features, such as deep-cut valleys and rock-seated terraces (Figure 10a), and the mountain debris was carried to the mountain front, the Awati fault depression and other low-lying areas with the water flow and deposited on the top of the alluvial-diluvial plain of the Aksu and Kekeya Rivers. Therefore, the sedimentary environment in this stage was characterized by fluvial facies and diluvial fan facies with sand and gravel, which had a good correspondence with the sudden rise in the rate of downcutting of the river where it exited near the mountain pass in this stage.

Stage II (climate warming period): After the last deglaciation period (LDP), the cold period slowly ended, the climate gradually warmed and the surface temperature gradually rose [91]. The upstream glacier retreated, the erosional base level of the river increased due to the rising river level, and the cutting rate slowed. Moreover, the upstream region carried a large amount of coarse-grained sediment into the middle and lower reaches of the river, and these sediments accumulated rapidly in the palaeochannels, and Class I terraces were formed. In the late LDP period, with the rapid rise in the river level and sedimentation, the palaeochannel was filled with fine-grained sediment (silty fine sand) owing to the weakening of hydrodynamic conditions, revealing that the paleogeographic environment gradually changed from fluvial facies to fluvial-lacustrine transitional facies. In addition, the rapid sediment accumulation in the riverway led to the formation of high and low riverbeds, whereas the low-lying land laid the foundation for the formation of lake groups (Figure 10c).

Stage III (warm-dry climate period): In the middle and late Holocene, the temperature started to warm, and the overall trend was a megathermal period, but there were several small local cooling events [92,93]. Simultaneously, due to the intensification of human activities, the climate was warm and dry, and the river level rose to the current level and gradually stabilized. During this period, lake groups developed significantly, and fine-grained unconsolidated sediments controlled by rivers and lakes formed a fine-grained plain area downstream (Figure 10e). The Holocene sedimentary layer in borehole AB06 was characterized by fluvial-lacustrine facies. In contrast, borehole AB04 exhibits fluvial facies sedimentation due to the influence of the Aksu River.

5.2. Evolutionary Pattern of the GFS since the LGM

The difference in the permeability in the aquiferous medium in the sedimentary lithofacies of different aquifer systems determines the distribution of different hierarchies of the GFS; thus, comprehensively analyzing the development of the paleogeographic environment forms the foundation for reconstructing the evolutionary pattern of the GFS. In addition, owing to the combined effects of westerly circulation-influenced climate fluctuations and tectonic uplift since the LGM [94,95], which have led to significant changes in river levels and erosional base levels in small- and medium-sized watersheds in the study area, this process regulates the groundwater driving force, which ultimately creates the various patterns of the GFS. Hence, according to the analysis of the above influencing factors, the evolutionary pattern of the GFS in the Aksu River Basin since the LGM also could essentially be broken down into three stages.

Stage I (intense downcutting period, 27–13 ka BP): At this stage, the whole shallow aquifer system had not yet formed, while the middle and deep aquifer systems were mainly dominated by coarse-grained sediments in the riverbed and floodplain microfacies

with good permeability. Due to the southern Tianshan overthrust nappe structure, the upper Aksu River was uplifted, the Class II terrace that had formed was uplifted, the river channel shifted to the left bank in the piedmont zone, the river entered a period of rapid downcutting (the downcutting rate reached 3.3 m/ka), the diluvial fan group extended in the runoff direction, and the base level of river erosion decreased. Additionally, the palaeoclimate entered the cold-dry stage, which resulted in a decrease in river flow and the formation of low water levels and low lake surfaces. The gravitational water potential difference in the Aksu River Basin extremely increased due to the headward erosion and low water level, and its groundwater driving force reached an extreme value (Figure 10b), which favored the formation and development of the regional GFS in the early period. In addition, according to the distribution of the existing groundwater ages, the age of the oldest groundwater in the Quaternary basin borehole dates back to nearly 24 ka, which directly proves that the GFS pattern revealed in the existing borehole had evolved from the LGM period, and the developmental groundwater flow had utterly penetrated the shallow and middle aquifer systems (approaching or reaching the maximum depth of borehole disclosure). Thus, after tens of thousands of years of cyclic evolution, the ages of groundwater in the local and intermediate GFS during this stage had not been retained to the present and had been completely replaced by newer groundwater.

Stage II (slow downcutting period, 13–8 ka BP): During this stage, YD events ended, the climate at that time gradually warmed, the downward erosion rate entered a slow period, and the water level of the Aksu River gradually rose, which significantly reduced the water potential difference and weakened the driving force of groundwater, resulting in many vertical coarse particle deposits (sedimentation rate of 0.7 m/ka) in the palaeochannel. The thick sand and gravel layer was formed in the intermontane basin, in the alluvial-diluvial inclined zone in front of the Gumubiezi Mountains and in the gravel plain area, and the middle coarse sand layer was formed in the downstream alluvial plain area. During the same period, the depth of recirculation of the regional GFS decreased to the top part of the deep aquifer system and tended to stagnate, which could be inferred from the age of groundwater in this layer (nearly 10 ka). Furthermore, the regional GFS that formed during the first stage was gradually buried deeper in the basin. In the plain area, the intermediate GFS began to develop due to the emergence of microtopography that favored accumulation. Simultaneously, the local GFS gradually formed in the intermontane basin and the alluvial-diluvial inclined zone in front of the Gumubiezi Mountains (Figure 10d).

Stage III (relatively stable period, 8 ka BP to present): The tectonic movement further weakened, the temperature zigzagged upwards, and the Holocene megathermal period (HMP) began. Persistent droughts led to massive glacial melting, and the river runoff increased, the water level rose, and the groundwater driving forces gradually stabilized at a dynamic equilibrium level. The regional GFS that formed during Stages I and II was preserved in a deep basin that maintained groundwater ages of 10–24 ka and was generally considered a stagnant system. Thus, the recirculation depth of the regional GFS in this stage only reached the bottom of the middle aquifer system, whereas the middle aquifer system had sufficiently circulated, causing the groundwater age to vary from 1–10 ka. These systems were considered stable systems based on the existing groundwater flow pattern. As rivers have fully developed and artificial reservoirs and water diversion channels have been constructed in the last 2 ka, the water potential difference between various hydrological units in the plain area has become the main force driving shallow groundwater flow (such as in rivers, lakes, and artificial canals). Correspondingly, rivers and inter-river low-lying lands (including reservoirs, natural lakes, etc.) are the potential water sources or sinks of each other, and these effects vary based on the season, leading to the formation of an active local GFS (groundwater age < 100 a) (Figure 10f).

Macroscopically, the top of the middle-late Pleistocene Wensu uplift began to receive deposition [96,97]; thus, surface rivers flowing through the Gumubiezi Mountains and groundwater of the alluvial-diluvial inclined zone pediment accumulated in the hinterland of the plain. The Yingan Mountains were gradually uplifted under the influence of the

Keping thrust belt [98–100], resulting in the decline of the southwest side of the study area, which caused the depositional center of the Awati fault depression to shift westwards and the basement to deepen. This process may have preserved the ultradeep aquifer system, which is not discussed in this paper because the borehole has not reached the bottom. With the frequent development of sinistral right-stepping strike-slip neotectonic movements, such as the Shajingzi fault, Aqia fault and Tumuxiuke fault [101–103], the Awati depression (block) rotated clockwise with respect to the geological bodies (Wenshu uplift, Tabei uplift and Bachu uplift) separated by the peripheral boundary of the large fault belt [104], thus forming ENE tensile stress. In addition, the HMP entered a persistent drought and warm climate, resulting in the trunk stream of the Aksu River swinging in stages and moving eastwards to the current position of the Laodahe and Xindahe branch streams; this process left several traces of river capture and riverway migration adjustment in the western alluvial plain; then, the rivers evolved into intermittent oxbow lakes, eventually forming a unified Aksu River.

At present, under the background of a warming climate and intensification of human activities, the evolution of watershed-scale groundwater flow systems has some new characteristics. Due to the overexploitation of groundwater and the abuse of organic fertilizer, the groundwater level decreased and organic pollutants increased, which further contributed to the dissolution and enrichment of high fluorine arsenic in the concentrated drainage zone of regional groundwater flow [105], and preemptively discharged downstream in the overflow zone of the watershed simultaneously, resulting in the migration of soil salting to the upstream. Due to the melting of glaciers in the upper mountain area, the sudden eruption of mountain floods is aggravated, and the available freshwater resources are released in advance downstream without slow seepage downward. Therefore, the construction of new water infrastructures can effectively prolong the storage utilization of water resources, increase the recharge of middle and deep groundwater flow, and restore the sustainable cycle of the basin ecology. It is expected that the research results can also be widely used in engineering construction to provide scientific site selection and safe drinking water source areas.

6. Conclusions

Through the detailed analysis of hydrogeological conditions, sediment particle size distribution, stratigraphic logging curve characteristics, sediment age, glacial sedimentary sequence, palaeoclimatic indicators and existing groundwater age in the Aksu River Basin, this paper reconstructs the sedimentary environment of the basin-scale aquifer system in the study area and constructs a complex coupling relationship between the palaeosedimentary environment, palaeoclimate and GFS in the basin, which scientifically reveals the pattern of GFS evolution driven by river level that was jointly controlled by climate change and neotectonic uplift movement in the Aksu River Basin. The major results are summarized below:

(1) During the evolution history of the sedimentary environment of the Quaternary aquifer system, the study area underwent at least seven stable-erosive periods, and the sedimentary facies were characterized by the diluvial fan and fluvial facies dominating in the upper reaches and fluvial, lacustrine, and fluvial-lacustrine transitional facies dominating in the middle and lower reaches. The sedimentary environment underwent a process from deep downcutting in the LGM to the deposition of fluvial facies with the rapid filling of coarse-grained sediments in the LDP period and then to the deposition of lacustrine facies with stable fine-grained sediments in the HMP. Moreover, the transition of the middle and deep aquifer system from coarse-grained facies to fine-grained facies in the shallow aquifer system was closely related to the fluctuation in the river level, showing that the hydrodynamic conditions were gradually weakened and tended to stabilize. The results showed that in the Aksu River Basin, there was a complex coupling relationship among the glacial sedimentary

sequence of the Tomur Peak area, climatic evolution, neotectonic movement and sedimentary facies of the foreland basin.

(2) Since the Quaternary, the climate around the Tarim Basin has had similar spatial and temporal evolutionary characteristics, and it can be divided into four stages: a cold-dry climate in the early Pleistocene, warm-humid climate in the middle Pleistocene, long-term dry-cold climate from the late Pleistocene to the Holocene, and warm-arid climate since the Holocene. The climatic evolution of the Aksu River Basin is basically consistent with that of the Tarim Basin; the basin responded to most of the global climate events from the LIA to MIS12, and the results demonstrate the gradual aridification process of the climate in the study area affected by the westerly circulation since the LGM.

(3) During the LGM, tectonic uplift and climate change controlled the strength of the driving forces of groundwater in the study area; and these results, combined with the existing groundwater age distribution in the Aksu River Basin, allowed the evolution of the GFS to be divided into three stages: an era of intense downscaling, followed by a phase of gradual downscaling, and finally a relatively stable period. Since Stages III, the regional GFSs that formed in Stages I and II were preserved in the deep basin, and the middle aquifer system was also fully circulated, both of which were considered stable systems. In the last 2.0 ka BP, as the river system has fully developed and artificial reservoirs and water diversion channels have been constructed, high and low riverbeds and inter-river low-lying lands interconnected with each other, as potential water sources or sinks depending on the season, which resulted in the formation of an active localized GFS.

This study not only advances our understanding of the evolution of the GFS in the Aksu River Basin of the arid inland basin, but also elucidates its complex connections with climate fluctuations and geological dynamics.

Author Contributions: Methodology, H.S.; Project administration and Supervision, Y.D., W.N. and R.Z.; Writing—original draft, H.S. and Y.D.; Visualization and Writing-review, J.H., P.L., H.Y., L.C. and N.W. All authors have read and agreed to the published version of the manuscript.

Funding: This research work was supported by the National Natural Science Foundation of China (No. 41172277) and Xinjiang Geological Exploration Fund (No. S15-2-LQ01 and No. S17-2-XJ06).

Data Availability Statement: Data will be made available on request.

Acknowledgments: The authors thank Yunsheng Wang, Xiaoping Gong, Sheng Li, Lihe Yin, Junbo Bi, Qiong Han, Zhanchao Pan, Xin Guo and Zongchang Wu for their valuable comments and suggestions. We also wish to thank the editor and reviewers for their constructive and insightful comments on the manuscript.

Conflicts of Interest: The authors declare no conflict of interest.

References

1. Wang, J.Z.; Jia, H.J. Sediment record of environmental change at Late Lop Nur (Xinjiang, NW China) from 13.0 to 5.6 cal ka BP. *Chin. J. Oceanol. Limnol.* **2017**, *35*, 1070–1078. [CrossRef]
2. Wang, C.S.; Hazen, R.M.; Cheng, Q.M.; Stephenson, M.H.; Zhou, C.H.; Fox, P.; Shen, S.Z.; Oberhansli, R.; Hou, Z.Q.; Ma, X.G.; et al. The Deep-Time Digital Earth program: Data-driven discovery in geosciences. *Natl. Sci. Rev.* **2021**, *8*, nwab027. [CrossRef]
3. Tóth, J. *Gross-Formational Gravity-Flow of Groundwater: A Mechanism of the Transport Accumulation of Petroleum (The Generalized Hydraulic Theory of Petroleum Migration) in Problems Migration*; Rober, W.H., III, Cordell, R.J., Eds.; AAPG Studies in Geology: Tulsa, OK, USA, 1980; pp. 121–167.
4. Edmunds, W.M.; Fellman, E.; Goni, I.B.; Prudhomme, C. Spatial and temporal distribution of groundwater recharge in northern Nigeria. *Hydrogeol. J.* **2002**, *10*, 205–215. [CrossRef]
5. Han, D.M.; Liang, X.; Currell, M.J.; Song, X.F.; Chen, Z.Y.; Jin, M.G.; Liu, C.M.; Han, Y. Environmental isotopic and hydrochemical characteristics of groundwater systems in Daying and Qicun geothermal fields, Xinzhou Basin, Shanxi, China. *Hydrol. Process.* **2010**, *24*, 3157–3176. [CrossRef]
6. Sorg, A.; Mosello, B.; Shalpykova, G.; Allan, A.; Hill Clarvis, M.; Stoffel, M. Coping with changing water resources: The case of the Syr Darya river basin in Central Asia. *Environ. Sci. Policy* **2014**, *43*, 68–77. [CrossRef]

7. Lei, M.; Zhou, J.L.; Zhou, Y.Z.; Sun, Y.; Ji, Y.Y.; Zeng, Y.Y. Spatial distribution, source apportionment and health risk assessment of inorganic pollutants of surface water and groundwater in the southern margin of Junggar Basin, Xinjiang, China. *J. Environ. Manag.* **2022**, *319*, 115757. [CrossRef] [PubMed]
8. Huo, Z.; Feng, S.; Kang, S.; Li, W.; Chen, S. Effect of climate changes and water-related human activities on annual stream flows of the Shiyang River basin in arid north-west China. *Hydrol. Process.* **2008**, *22*, 3155–3167. [CrossRef]
9. Wang, G.Y.; Shen, Y.P.; Zhang, J.G.; Wang, S.D.; Mao, W.Y. The effects of human activities on oasis climate and hydrologic environment in the Aksu River Basin, Xinjiang, China. *Environ. Earth Sci.* **2010**, *59*, 1759–1769. [CrossRef]
10. Dong, W.; Cui, B.; Liu, Z.; Zhang, K. Relative effects of human activities and climate change on the river runoff in an arid basin in northwest China. *Hydrol. Process.* **2014**, *28*, 4854–4864. [CrossRef]
11. Tóth, J. A theoretical analysis of groundwater flow in small drainage basins. *J. Geophys. Res.* **1963**, *68*, 4795–4812. [CrossRef]
12. Engelen, G.B.; Jones, G.P. Developments in the analysis of groundwater flow systems. *Int. Assoc. Hydrol. Sci.* **1986**, *163*, 2–8.
13. Toth, J. *Gravitational System of Groundwater: Theory, Evaluation, Utilization*; Cambridge University Press: New York, NY, USA, 2009; p. 297.
14. Liang, X.; Zhang, R.Q.; Jin, M.G. *Groundwater Flow Systems: Theory, Application and Investigation*; Geological Publishing House: Beijing, China, 2015; p. 24. (In Chinese)
15. Inbar, N.; Rosenthal, E.; Magri, F.; Alraggad, M.; Moller, P.; Flexer, A.; Guttman, J.; Siebert, C. Faulting patterns in the Lower Yarmouk Gorge potentially influence groundwater flow paths. *Hydrol. Earth Syst. Sci.* **2019**, *23*, 763–771. [CrossRef]
16. Zhang, Z.G.; Shi, D.H.; Ren, F.H.; Yin, Z.Z.; Sun, J.C.; Zhang, C.Y. Evolution of Quaternary groundwater system in North China Plain. *Sci. China (Ser. D)* **1997**, *40*, 276–283. [CrossRef]
17. Zhang, R.Q.; Liang, X.; Jin, M.G. The evolution of groundwater flow systems in the Quaternary of Hebei Plain since the last glacial maximum. *Earth Sci. Front.* **2013**, *20*, 217–226, (In Chinese, with English Abstract).
18. Liang, X.; Zhang, J.W.; Lan, K.; Shen, S.; Ma, T. Hydrochemical characteristics of groundwater and analysis of groundwater flow systems in Jianghan Plain. *Bull. Geol. Sci. Technol.* **2020**, *39*, 21–33, (In Chinese, with English Abstract).
19. Zhang, J.W.; Liang, X.; Jin, M.G.; Li, J.; Shen, S.; Wang, L.X.; Ma, T. Evolution of the groundwater flow system driven by the sedimentary environment since the Last Glacial Maximum in the central Yangtze River Basin. *J. Hydrol.* **2022**, *610*, 127997. [CrossRef]
20. Sun, D.H.; Bloemendal, J.; Yi, Z.Y.; Zhu, Y.H.; Wang, X.; Zhang, Y.B.; Li, Z.J.; Wang, F.; Han, F.; Zhang, Y. Palaeomagnetic and palaeoenvironmental study of two parallel sections of late Cenozoic strata in the central Taklimakan Desert: Implications for the desertification of the Tarim Basin. *Palaeogeogr. Palaeoclimatol. Palaeoecol.* **2011**, *300*, 1–10. [CrossRef]
21. Bi, Z.W.; Yang, Z.J.; Xu, J.M.; Song, S.H.; Hou, H.B.; Chen, J. Grain-size characteristics and sediment environment of Quatenary sediments in the central Tarim basin. *Arid Land Geogr.* **2009**, *32*, 335–339, (In Chinese, with English Abstract).
22. Xu, J.M.; Yang, Z.J.; Bi, Z.W.; Guo, X.H.; Zhang, J.P.; Zhang, H.R. Carbon, oxygen isotopic characteristic and their paleoenvironment significance from Quaternary sediment in the Tarim basin. *J. Eng. Geol.* **2007**, *15* (Suppl. S1), 50–54. (In Chinese, with English Abstract)
23. Bai, Y.L.; Wang, J.R.; Tian, K.; Wang, D.Q.; Zhao, N. Element geochemistry characteristic from the 72-51 ka BP lake sediments in the northern margin of Kongqi River, Xinjiang. *Arid Land Geogr.* **2016**, *39*, 477–485. (In Chinese, with English Abstract)
24. Su, J.; Liu, Y.X.; Bai, Y.L. Grain size characteristics of late Pleistocene lacustrine sediments in eastern Tarim Basin and their paleoenvironmental significance. *West-China Explor. Eng.* **2017**, *1*, 157–164. (In Chinese, with English Abstract)
25. Sun, Z.C.; Feng, X.J.; Li, D.M.; Yang, F.; Qu, Y.H.; Wang, H.J. Cenozoic Ostracoda and palaeoenvironments of the northeastern Tarim Basin, western China. *Palaeogeogr. Palaeoclimatol. Palaeoecol.* **1999**, *148*, 37–50. [CrossRef]
26. Luo, C.; Peng, Z.C.; Yang, D.; Liu, W.G.; Zhang, Z.F.; He, J.F.; Chou, C.N. A lacustrine record from Lop Nur, Xinjiang, China: Implications for paleoclimate change during Late Pleistocene. *J. Asian Earth Sci.* **2009**, *34*, 38–45.
27. Yan, S.; Qin, X.Y. Quaternary environmental evolution of the Lop Nur region, NW China. *Acta Micropalaeontol. Sin.* **2000**, *17*, 165–169.
28. Yan, F.H.; Ye, Y.Y.; Mai, X. The sporo-pollen assemblage in the luo 4 drilling of Lop Lake in Uygur autonomus region of Xinjiang and its significance. *Seisimol. Geol.* **1983**, *5*, 75–81, (In Chinese, with English Abstract).
29. Wang, C.S.; Wang, T.T.; Chen, X.; Gao, Y.; Zhang, L.M. Paleoclimate implications for future climate change. *Earth Sci. Front.* **2017**, *24*, 1–17, (In Chinese, with English Abstract).
30. Lin, J.X.; Zhang, J.; Ju, Y.J.; Wang, Y.; Lin, F.; Zhang, J.P.; Wang, S.F.; Wei, M.R. The lithostratigrapuy, magnetostratigraphy, and climatostratigraphy in the Lop Nur region, Xinjiang. *J. Stratigr.* **2005**, *29*, 317–322.
31. Zhang, R.; Li, L.; Nai, W.H.; Gu, Y.S.; Huang, C.J.; Ogg, J.; Li, Q.H.; Lu, C.X.; Wang, Z.X. Astronomical forcing of terrestrial climate recorded in the Pleistocene of the western Tarim Basin, NW China. *Palaeogeogr. Palaeoclimatol. Palaeoecol.* **2019**, *530*, 78–89. [CrossRef]
32. Zhang, R.; Yin, Q.Z.; Nai, W.H.; Wang, Z.X.; Lu, H.; Huang, C.J.; Gu, Y.S.; Li, L.; Wang, Y.S.; Liu, L.J. Orbital and Millennial-Scale Climate Variability over the Past 76 ka in the Western Tarim Basin, Northwest China. *J. Earth Sci.* **2023**, *34*, 173–180. [CrossRef]
33. Head, M.J. Formal subdivision of the Quaternary System/Period: Present status and future directions. *Quat. Int.* **2019**, *500*, 32–51. [CrossRef]
34. Chen, F.H.; Chen, J.H.; Huang, W. A discussion on the westerly-dominated climate model in mid-latitude Asia during the modern interglacial period. *Earth Sci. Front.* **2009**, *16*, 23–32. (In Chinese) [CrossRef]

35. Xu, J.H.; Chen, Y.N.; Lu, F.; Li, W.H.; Zhang, L.J.; Hong, Y.L. The nonlinear trend of runoff and its response to climate change in the Aksu River, western China. *Int. J. Climatol.* **2011**, *31*, 687–695. [CrossRef]
36. Fan, Y.T.; Chen, Y.N.; Li, W.H. Increasing precipitation and baseflow in Aksu River since the 1950s. *Quat. Int.* **2014**, *336*, 26–34. [CrossRef]
37. Liu, S.Y.; Ding, Y.J.; Shangguan, D.H. Glacier retreat as a result of climate warming and increased precipitation in the Tarim River Basin, Northwest China. *Ann. Glaciol.* **2006**, *43*, 91–96. [CrossRef]
38. Feng, S.; Hu, Q.; Huang, W.; Ho, C.H.; Li, R.; Tang, Z. Projected climate shift under future global warming from multi-model, multi-scenario, CMIP5 simulations. *Glob. Planet. Change* **2014**, *112*, 41–52. [CrossRef]
39. Chen, F.H.; Yu, Z.C.; Yang, M.L.; Ito, E.; Wang, S.M.; Madsen, D.B.; Huang, X.Z.; Zhao, Y.; Sato, T.; Birks, H.J.B.; et al. Holocene moisture evolution in arid central Asia and its out-of-phase relationship with Asian monsoon history. *Quat. Sci. Rev.* **2008**, *27*, 351–364. [CrossRef]
40. Pan, Y.X.; Dai, S.E. *Report of 1:200,000 Regional Hydrogeological Survey in Aksu Prefecture, Xinjiang*; Xinjiang Geological Archive: Urumqi, China, 1979.
41. Blatt, H. *Sedimentary Petrology*; Freeman W H and Company: New York, NY, USA, 1982; p. 564.
42. Yuan, H.Q.; Wang, L.; Yu, Y.H.; Zhang, D.J.; Xu, F.M.; Liu, H.T. Review of sedimentary grain size analysis methods. *J. Jilin Univ. (Earth Sci. Ed.)* **2019**, *49*, 380–393.
43. Wang, Z.M.; Long, H.S. Different hydrocarbon accumulation histories in the Kelasu-Yiqikelike structural belt of the Kuqa foreland basin. *Acta Geol. Sin. Engl. Ed.* **2010**, *84*, 1195–1208.
44. Wen, L.; Li, Y.J.; Zhang, G.Y.; Zhang, G.Y.; Tian, Z.J.; Peng, G.X.; Qiu, B.; Huang, Z.B.; Luo, J.C.; Zhang, Q. Evolution of fold-thrust belts and Cenozoic uplifting of the South Tianshan Mountain range in the Kuqa region, Northwest China. *J. Asian Earth Sci.* **2017**, *135*, 327–337. [CrossRef]
45. Neng, Y.; Xie, H.W.; Yin, H.W.; Li, Y.; Wang, W. Effect of basement structure and salt tectonics on deformation styles along strike: An example from the Kuqa fold–thrust belt, West China. *Tectonophysics* **2018**, *730*, 114–131. [CrossRef]
46. Zhang, J.F.; Zhang, Y.Y.; Gao, Y.J. Silurian hydrocarbon exploration breakthrough and its implications in the Shajingzi structural belt of Tarim Basin, NW China. *Pet. Explor. Dev.* **2022**, *49*, 233–246. [CrossRef]
47. Turner, S.A.; Cosgrove, J.W.; Liu, J.G. Controls on lateral structural variability along the Keping Shan Thrust Belt, SW TianShan Foreland, China. *Geol. Soc. Lond. Spec. Publ.* **2010**, *348*, 71–85. [CrossRef]
48. Chen, Z.L.; Wang, Z.X.; Han, F.B.; Zhang, W.G.; Zhang, Q.; Zhou, Z.J.; Wang, X.H.; Xiao, W.F.; Han, S.Q.; Zhou, Z.J.; et al. Late Cretaceous–Cenozoic uplift, deformation, and erosion of the SW Tianshan Mountains in Kyrgyzstan and Western China. *Int. Geol. Rev.* **2018**, *60*, 1019–1037. [CrossRef]
49. Zhao, J.D. *Preliminary Study on Evolution Sequence of Quaternary Glaciers in Jengish Chokusu Area*; Tianshan MountainsProQuest Digital Dissertations; South China Normal University: Guangzhou, China, 2007; (In Chinese, with English Abstract).
50. Jia, Y.; Shi, Y.; Wang, S.; Jiang, X.; Li, S.; Wang, A.; Li, X. Lake expanding events in the Tibetan Plateau since 40 kaBP. *Sci. China (Ser. D)* **2001**, *44* (Suppl. S1), 301–315. [CrossRef]
51. Zhang, H.C.; Wunnemann, B.; Ma, Y.Z.; Peng, J.L.; Pachur, H.; Li, J.J.; Qi, Y.; Chen, G.J.; Fang, H.B.; Feng, Z.D. Lake level and climate changes between 42000 and 18000 ^{14}C yr BP in the Tengger Desert, northwestern China. *Quat. Res.* **2002**, *58*, 62–72. [CrossRef]
52. Yang, B.; Shi, Y.F. Warm-humid climate in Northwest China during the period of 40-30ka BP: Geological records and origin. *Quat. Sci.* **2003**, *23*, 60–68, (In Chinese, with English Abstract).
53. Zhao, J.D.; Liu, S.Y.; He, Y.Q.; Song, Y.G. Quaternary glacial chronology of the Ateaoyinake River Valley, Tianshan Mountains, China. *Geomorphology* **2009**, *103*, 276–284. [CrossRef]
54. Zhao, J.; Song, Y.; King, J.W.; Liu, S.; Wang, J.; Wu, M. Glacial geomorphology and glacial history of the Muzart River valley, Tianshan Range, China. *Quat. Sci. Rev.* **2010**, *29*, 1453–1463. [CrossRef]
55. Zhao, J.D.; Liu, S.Y.; He, Y.Q.; Deng, X.F.; ShangGuan, D.H. The Glacial Sediments Sequences in the Ateaoyinake River Valley, Tianshan Mountains. *Acta Geogr. Sin.* **2006**, *61*, 491–500.
56. He, M.L.; Xu, M.; Zhang, Q.; Zhao, X.; Ren, R. Preliminary study on valley variation in the mountain pass of Kumalake River of South Tianshan Mountain since the Quaternary. *South-North Water Sci. Technol.* **2013**, *11*, 62–66. (In Chinese, with English Abstract)
57. Folk, R.L.; Ward, W.C. Brazos River bar: A study in the significance of grain size parameters. *J. Sediment. Petrol.* **1957**, *27*, 3–26. [CrossRef]
58. Wang, Y.N.; Li, S.; Yu, B. Spatial variability analysis of permeability coefficient in Aksu River Basin. *China Rural Water Hydropower* **2021**, *1*, 64–75, (In Chinese, with English Abstract).
59. Lisa, C.; Or, M.B.; Zvi, B.; Michael, L. Late Quaternary lacustrine deposits of the Dead Sea basin: High resolution sequence stratigraphy from downhole logging data. *Quat. Sci. Rev.* **2019**, *210*, 175–189.
60. Shi, Y.F.; Zheng, B.X.; Su Zhen Mu, Y.Z. Study of Quaternary glaciation in Mts. Tomur-Hantengri area, Tianshan. *J. Glaciol. Geocryol.* **1984**, *6*, 1–14, (In Chinese, with English Abstract).
61. Kukla, G.; Heller, F.; Liu, X.M.; Xu, T.C.; Liu, T.S.; An, Z.S. Pleistocene climate in China dated by magnetic susceptibility. *Geology* **1988**, *16*, 811–814. [CrossRef]
62. Gallet, S.; Jahn, B.; Torii, M. Geochemical characterization of the Luochuan loess-paleosol sequence, China, and paleoclimatic implications. *Chem. Geol.* **1996**, *133*, 67–88. [CrossRef]

63. Wang, Z.; Xu, H.; Zhan, Q.; Saito, Y.; He, Z.; Xie, J.; Li, X.; Dong, Y. Lithological and Palynological Evidence of Late Quaternary Depositional Environments in the Subaqueous Yangtze Delta, China. *Quat. Res.* **2010**, *73*, 550–562. [CrossRef]
64. Nai, W.H.; Li, B.; Chang, Z.Y.; Wang, Y.X.; Han, Y.J.; Tian, Y.N. *Report on 1:100,000 Hydrogeological and Environmental Geological Survey of the Kashgar Delta, Xinjiang*; No.2 Hydrogeological and Engineering Geological Team, Xinjiang Bureau of Geology and Mineral Resources Exploration and Development: Urumqi, China, 2018. (In Chinese)
65. Heinrich, H. Origin and Consequences of Cyclic Ice Rafting in the Northeast Atlantic Ocean during the Past 130,000 Years. *Quat. Res.* **1988**, *29*, 142–152. [CrossRef]
66. Bond, G.; Broecker, W.; Johnsen, S.; McManus, J.; Labeyrie, L.; Jouzel, J.; Bonani, G. Correlations between Climate Records from North Atlantic Sediments and Greenland Ice. *Nature* **1993**, *365*, 143–147. [CrossRef]
67. Huang, X.Z.; Chen, F.H.; Fan, Y.X.; Yang, M.L. Dry late-glacial and early Holocene climate in arid central Asia indicated by lithological and palynological evidence from Bosten Lake, China. *Quat. Int.* **2009**, *194*, 19–27. [CrossRef]
68. Li, Y.; Song, Y.G.; Lai, Z.P.; Han, Z.P.; Han, L.; An, Z.S. Rapid and Cyclic Dust Accumulation during MIS 2 in Central Asia Inferred from Loess OSL Dating and Grain-Size Analysis. *Sci. Rep.* **2016**, *6*, 32365. [CrossRef] [PubMed]
69. Liu, X.K.; Chen, J.H.; Chen, S.Q.; Wang, H.P.; Huang, W.; Feng, S.; Chen, F.H. Abrupt climate change in arid central Asia during the Holocene: A review. *Earth-Sci. Rev.* **2023**, *242*, 104450. [CrossRef]
70. Lifton, N.; Beel, C.; Haattestrand, C.; Kassab, C.; Rogozhina, I.; Heermance, R.; Oskin, M.; Burbank, D.; Blomdin, R.; Gribenski, N.; et al. Constraints on the late Quaternary glacial history of the Inylchek and Sary-Dzaz valleys from in situ cosmogenic ^{10}Be and ^{26}Al, eastern Kyrgyz Tian Shan. *Quat. Sci. Rev.* **2014**, *101*, 77–90. [CrossRef]
71. NGRIP Members (North Greenland Ice Core Project Members). High-Resolution Record of Northern Hemisphere Climate Extending into the Last Interglacial Period. *Nature* **2004**, *431*, 147–151. [CrossRef]
72. Yao, S.D.; Xu, B.Q.; Pu, J.C. Climate change on orbital and suborbital timescales recorded by the Guliya ice core in the Tibetan Plateau. *Sci. China (Ser. D)* **2001**, *31*, 287–294. (In Chinese)
73. Sun, Y.B.; Clemens, S.C.; Morrill, C.; Lin, X.P.; Wang, X.L.; An, Z.S. Influence of Atlantic Meridional Overturning Circulation on the East Asian Winter Monsoon. *Nat. Geosci.* **2012**, *5*, 46–49. [CrossRef]
74. Huang, W.; Chen, J.H.; Zhang, X.J.; Feng, S.; Chen, F.H. Definition of the core zone of the "westerlies-dominated climatic regime", and its controlling factors during the instrumental period. *Sci. China Earth Sci.* **2015**, *58*, 676–684. [CrossRef]
75. Mix, A.C.; Bard, E.; Schneider, R. Environmental processes of the ice age: Land, oceans, glaciers. *Quat. Sci. Rev.* **2001**, *20*, 627–657. [CrossRef]
76. Clark, P.U.; Dyke, A.S.; Shakun, J.D.; Carlson, A.E.; Clark, J.; Wohlfarth, B.; Mitrovica, J.X.; Hostetler, S.W.; McCabe, A.M. The last glacial maximum. *Science* **2009**, *325*, 710e714. [CrossRef]
77. Hughes, P.D.; Gibbard, P.L.; Ehlers, J. Timing of glaciation during the last glacial cycle: Evaluating the concept of a global 'Last Glacial Maximum' (LGM). *Earth Sci. Rev.* **2013**, *125*, 171e198. [CrossRef]
78. Feng, Q.; Su, Z.Z.; Jin, H.J. Study on desert evolution and climate change in Tarim River Basin since 12 kaBP. *Sci. China (Ser. D)* **1999**, *42*, 101–112. [CrossRef]
79. Wünnemann, B.; Mischke, S.; Chen, F.H. A Holocene sedimentary record from Bosten Lake, China. *Palaeogeogr. Palaeoclimatol. Palaeoecol.* **2006**, *234*, 223–238. [CrossRef]
80. Zhong, W.; Tueerxun, K.; Shu, Q.; Wang, L.G. Paleoclimatic and Paleoenvironmental evolution since about 25 ka BP in the Taitema Lake area, south Xinjiang. *Arid. Geogr.* **2005**, *28*, 183–187, (In Chinese, with English Abstract).
81. Li, Y.; Morrill, C. Multiple factors causing Holocene lake-level change in monsoonal and arid central Asia as identified by model experiments. *Clim. Dyn.* **2010**, *35*, 1119–1132. [CrossRef]
82. Zhang, R. Orbital and Millennial-Scale Climate Changes during the Middle Pleistocene from Western Tarim Basin, Northwest China, ProQuest Digital Dissertations, CNKI, Beijing, China, 2020. (In Chinese, with English Abstract).
83. Xiao, J.; Liu, G.N.; Nie, Z.Y.; Chen, Y.X.; Peng, X.; Liu, B.B.; Han, Y.S.; Cui, Z.J. Glacial evidence of aridification in the Tianshan Mountains since the Last Glacial. *J. Glaciol. Geocryol.* **2018**, *40*, 434–447, (In Chinese, with English Abstract).
84. Liu, J.L.; Guo, X.G.; Chen, D.L.; Li, J.; Yue, B.S.; Zeng, X.M. Diversification and historical demography of the rapid racerunner (*Eremias velox*) in relation to geological history and Pleistocene climatic oscillations in arid Central Asia. *Mol. Phylogenetics Evol.* **2019**, *130*, 244–258. [CrossRef]
85. Yu, B. The Research on Groundwater Circulation in the Aksu River Basin Based on Isotope Technology, ProQuest Digital Dissertations, CNKI, Beijing, China, 2021. (In Chinese with English Abstract).
86. Fu, B.H.; Lin, A.M.; Kano, K.; Maruyama, T.; Guo, J.M. Quaternary folding of the eastern Tian Shan, northwest China. *Tectonophysics* **2003**, *369*, 79–101. [CrossRef]
87. Yang, X.P.; Ran, Y.K.; Chen, J.W.; Chen, L.C.; Xu, X.W. Terrace deformation measurement and crustal shortening of several new fold belts in Keping nappe structure. *Sci. China (Ser. D)* **2006**, *36*, 905–913.
88. Hubert-Ferrari, A.; Suppe, J.; Gonzalez-Mieres, R.; Wang, X. Mechanisms of active folding of the landscape (southern Tian Shan, China). *J. Geophys. Res.* **2007**, *112*, B03S09. [CrossRef]
89. Loury, Y.; Rolland, S.; Guillot, A.V.; Mikolaichuk, P.; Lanari, O.; Bruguier, O.; Bosch, D. Crustal-scale structure of South Tian Shan: Implications for subduction polarity and Cenozoic reactivation. In *Geological Evolution of Central Asian Basins and the Western Tian Shan Range Geological Society*; Brunet, M.-F., McCann, T., Sobel, E.R., Eds.; Special Publications: London, UK, 2015; Volume 424, pp. 1–31.

90. Wu, C. *Landform Environment Evolution of North China*; Science Press: Beijing, China, 2008. (In Chinese)
91. Osman, M.B.; Tierney, J.E.; Zhu, J.; Tardif, R.; Hakim, G.J.; King, J.; Poulsen, C.J. Globally resolved surface temperatures since the Last Glacial Maximum. *Nature* **2021**, *599*, 239–244. [CrossRef]
92. Mischke, S.; Wünnemann, B. The Holocene salinity history of Bosten Lake (Xinjiang, China) inferred from ostracod species assemblages and shell chemistry: Possible palaeoclimatic implications. *Quatern Int.* **2006**, *154–155*, 100–112. [CrossRef]
93. Zhang, C.; Feng, Z.; Yang, Q.; Gou, X.; Sun, F. Holocene environmental variations recorded by organic-related and carbonate-related proxies of the lacustrine sediments from Bosten Lake, northwestern China. *Holocene* **2010**, *20*, 363–373. [CrossRef]
94. Gong, Z.; Li, S.H.; Li, B. The evolution of a terrace sequence along the Manas River in the northern foreland basin of Tian Shan, China, as inferred from optical dating. *Geomorphology* **2014**, *213*, 201–212. [CrossRef]
95. Wu, C.Y.; Alimujiang Dai, X.Y.; Wu, G.D.; Chen, J.B. Discovery of the Late-Quaternary activity along the eastern segment of maidan fault in southwest Tianshan and its tectonic implication. *Seismol. Geol.* **2014**, *36*, 976–990. (In Chinese, with English Abstract)
96. Yang, Y.X.; Gao, Y.J.; Zhang, J.F.; Zhou, X.G.; Zhang, J.H.; Miao, M.Q. New understanding of petroleum geological conditions of Wensu bulge in Tarim Basin, Xinjiang. *Geol. Surver China* **2019**, *6*, 11–16. (In Chinese, with English Abstract)
97. Zhang, J.H.; Yang, Y.X.; Gao, Y.J.; Li, S.M.; Yu, B.S.; Yu, B.S.; Gong, X.X.; Bai, Z.K.; Miao, M.Q.; Zhang, Y.Y.; et al. Geochemistry and source of crude oils in the Wensu uplift, Tarim Basin, NW China. *J. Pet. Sci. Eng.* **2022**, *208*, 109448. [CrossRef]
98. Yin, A.; Nie, S.; Craig, P.; Harrison, T.M.; Ryerson, F.J.; Qian, X.L.; Yang, G. Late Cenozoic tectonic evolution of the southern Chinese Tian Shan. *Tectonics* **1998**, *17*, 1–27. [CrossRef]
99. Yang, X.P.; Ran, Y.K.; Cheng, J.W.; Chen, L.C.; Xu, W. Measurement of terrace deformation and crustal shortening of some renascent fold zones within Kalpin nappe structure. *Sci. China Ser. D Earth Sci.* **2007**, *50*, 33–42. [CrossRef]
100. Liu, J.M.; Wang, Q.; Nie, X.H.; Gao, G.; Zhang, L.L.; Zhang, Z.G.; Xiang, Y. Analysis on the Characteristics of the Kalpin M_S5. 3 Earthquake Sequence of December 1, 2013, and Anomalies before the Earthquake. *Earthq. Res. China* **2017**, *31*, 381–394.
101. Li, J.Y.; Zhang, Q.; Zhang, G.Y.; Yang, H.J.; Yang, X.Z.; Shi, J.; Neng, Y.; Chen, Y.G.; Wen, L. Late Cenozoic trans-tensional fault belt discovered on the boundary of the Await Sag in the northwestern Tarin Basin. *Int. J. Earth Sci. (Geol. Rundsch.)* **2015**, *104*, 1253–1265. [CrossRef]
102. Wu, C.Y. Late Quaternary Activity of the East-Northeastern Trending Faults in the Southwestern Tianshan and Their Role in the Tectonic Deformation of the Tianshan Mountains. Ph.D. Thesis, Institute of Geology, China Earthquake Administration, Beijing, China, 2016.
103. Bai, Z.K.; Lu, X.X.; Song, Z.X.; Qiu, H.J.; Zhou, X.G.; Gao, Y.J.; Qi, Y.M.; Zhu, L.C.; Fu, X.T.; Zhou, Y.Y. Characteristics of boundary fault systems and its hydrocarbon controlling on hydrocarbon accumulation in Awati Sag, Tarim Basin, China. *China Geol.* **2019**, *2*, 94–107. [CrossRef]
104. Li, Y.J.; Sun, L.D.; Yang, H.J.; Zhang, G.Y.; Qi, Y.M.; Sang, H.; Wang, Y.R.; Liu, Y.L.; Zhang, Q.; Wen, L. The Late Cenozoic tensor-shear fault zones around Awati Sag, NW Tarim Basin. *Chin. J. Geol.* **2013**, *48*, 109–123. (In Chinese, with English Abstract)
105. McArthur, J.M.; Banerjee, D.M.; Hudson-Edwards, K.A.; Mishra, R.; Purohit, R.; Ravenscroft, P.; Cronin, A.; Howarth, R.J.; Chatterjee, A.; Talukder, T.; et al. Natural organic matter in sedimentary basins and its relation to arsenic in anoxic groundwater: The example of West Bengal and its worldwide implications. *Appl. Geochem.* **2004**, *19*, 1255–1293. [CrossRef]